1521-009X/48/12/1350–1363$35.00
DRUG METABOLISM AND DISPOSITION

https://doi.org/10.1124/dmd.120.000171
Drug Metab Dispos 48:1350–1363, December 2020

In Vitro Characterization of Ertugliflozin Metabolism by UDP-Glucuronosyltransferase and Cytochrome P450 Enzymes

Kimberly Lapham, Ernesto Callegari, Julie Cianfrogna, Jian Lin, Mark Niosi, Christine C. Orozco, Raman Sharma, and Theunis C. Goosen

Medicine Design, Pfizer Inc., Groton, Connecticut (K.L., E.C., J.L., M.N., C.C.O., R.S., T.C.G.) and Pfizer Inc., La Jolla, California (J.C.)

Received July 6, 2020; accepted September 22, 2020

ABSTRACT

Ertugliflozin is primarily cleared through UDP-glucurosyltransferase (UGT)–mediated metabolism (86%) with minor oxidative clearance (12%). In vitro phenotyping involved enzyme kinetic characterization of UGTs or cytochrome P450 enzymes catalyzing formation of the major 3-*O*-β-glucuronide (M5c) and minor 2-*O*-β-glucuronide (M5a), monohydroxylated ertugliflozin (M1 and M3), and des-ethyl ertugliflozin (M2) metabolites in human liver microsomes (HLMs). Fractional clearance (f_{CL}) from HLM intrinsic clearance (CL_{int}) indicated a major role for glucuronidation (f_{CL} 0.96; CL_{int} 37 μl/min per milligram) versus oxidative metabolism (f_{CL} 0.04; CL_{int} 1.64 μl/min per milligram). Substrate concentration at half-maximal velocity (K_m), maximal rate of metabolism (V_{max}), and CL_{int} for M5c and M5a formation were 10.8 μM, 375 pmol/min per milligram, and 34.7 μl/min per milligram and 41.7 μM, 94.9 pmol/min per milligram, and 2.28 μl/min per milligram, respectively. Inhibition of HLM CL_{int} with 10 μM digoxin or tranilast (UGT1A9) and 3 μM 16β-phenyllongifolol (UGT2B7/UGT2B4) resulted in fraction metabolism (f_m) estimates of 0.81 and 0.19 for UGT1A9 and UGT2B7/UGT2B4, respectively. Relative activity factor scaling of recombinant enzyme kinetics provided comparable f_m for UGT1A9 (0.86) and UGT2B7 (0.14). K_m and V_{max} for M1, M2, and M3 formation ranged 73.0–93.0 μM and 24.3–116 pmol/min per milligram, respectively, and was inhibited by ketoconazole (M1, M2, and M3) and montelukast (M2). In summary, ertugliflozin metabolism in HLMs was primarily mediated by UGT1A9 (78%) with minor contributions from UGT2B7/UGT2B4 (18%), CYP3A4 (3.4%), CYP3A5 (0.4%), and CYP2C8 (0.16%). Considering higher ertugliflozin oxidative metabolism (f_{CL} 0.12) obtained from human mass balance, human systemic clearance is expected to be mediated by UGT1A9 (70%), UGT2B7/UGT2B4 (16%), CYP3A4 (10%), CYP3A5 (1.2%), CYP2C8 (0.5%), and renal elimination (2%).

SIGNIFICANCE STATEMENT

This manuscript describes the use of orthogonal approaches (i.e., enzyme kinetics, chemical inhibitors, and recombinant enzymes) to characterize the fraction of ertugliflozin metabolism through various UDP-glucuronosyltransferase (UGT) and cytochrome P450 (CYP) enzyme-mediated pathways. Phenotyping approaches routinely used to characterize CYP hepatic fractional metabolism (f_m) to estimate specific enzymes contributing to overall systemic clearance were similarly applied for UGT-mediated metabolism. Defining the in vitro metabolic disposition and f_m for ertugliflozin allows risk assessment when considering potential victim-based drug-drug interactions perpetrated by coadministered drugs.

Introduction

Ertugliflozin (Fig. 1) is an orally administered, potent, and selective sodium-dependent glucose cotransporter (SGLT) 2 inhibitor (Mascitti et al., 2011) approved for the treatment of adults with type 2 diabetes mellitus (T2DM) at single daily doses of 5 or 15 mg as either monotherapy, fixed-dose combinations with metformin or sitagliptin, or in combination with antidiabetic medications (https://www.accessdata.fda.gov/scripts/cder/daf/index.cfm?event=overview.process&applno=209803; http://www.ema.europa.eu/ema/index.jsp?curl=pages/medicines/human/medicines/004315/human_med_002241.jsp&mid=WC0b01ac058001d124; Markham, 2018). Diabetes mellitus is a highly prevalent disease; there are approximately 463 million adults living with diabetes mellitus in 2019, a number expected to rise to 700 million by 2045 (https://www.idf.org/aboutdiabetes/what-is-diabetes/facts-figures.html). According to the National Diabetes Statistics Report from 2020, 34.2 million people in the United States have T2DM, of whom 7.3 million are undiagnosed (https://www.cdc.gov/diabetes/data/statistics/statistics-report.html). SGLT2 inhibitors such as ertugliflozin are indicated to treat T2DM as an adjunct to diet and exercise to improve glycemic control through inhibition of glucose reabsorption in the kidneys (Terra et al., 2017). Glucose homeostasis in the kidney is maintained by SGLT1, SGLT2, and SGLT3 transporters located in the brush border of the epithelial cells of proximal renal tubules (Wright, 2001). SGLT2 is the primary transporter responsible for glucose reabsorption (80%–90%) with a lesser role of SGLT1 (10%–20%), substantiated by compelling clinical data (Plosker, 2014; Deeks and Scheen, 2017; Frampton, 2018), preclinical investigation (Freitas et al., 2008; Han et al., 2008), and in vitro human kidney experiments (Hummel et al., 2011; Ghezzi and Wright, 2012; Vrhovac et al., 2015). Ertugliflozin is >2000-fold more selective as a SGLT2 inhibitor over SGLT1 (Mascitti et al., 2011). After a 5 or 15 mg once daily dose of ertugliflozin for 26 weeks to subjects with T2DM demonstrating inadequate glycemic control despite diet and exercise, fasting plasma

This study was sponsored by Pfizer Inc., New York, NY in collaboration with Merck Sharp & Dohme Corp., a subsidiary of Merck & Co., Inc., Kenilworth, NJ.

A portion of this work was presented as a poster at the *22nd North American International Society for the Study of Xenobiotics Meeting;* (2018) in Montréal, Canada.

L.P., E.C., J.C., J.L., M.N., C.C.O., R.S., and T.C.G. are employees of Pfizer Inc., New York, NY and may own shares/stock options in Pfizer Inc., New York, NY.

https://doi.org/10.1124/dmd.120.000171.

This article has supplemental material available at dmd.aspetjournals.org.

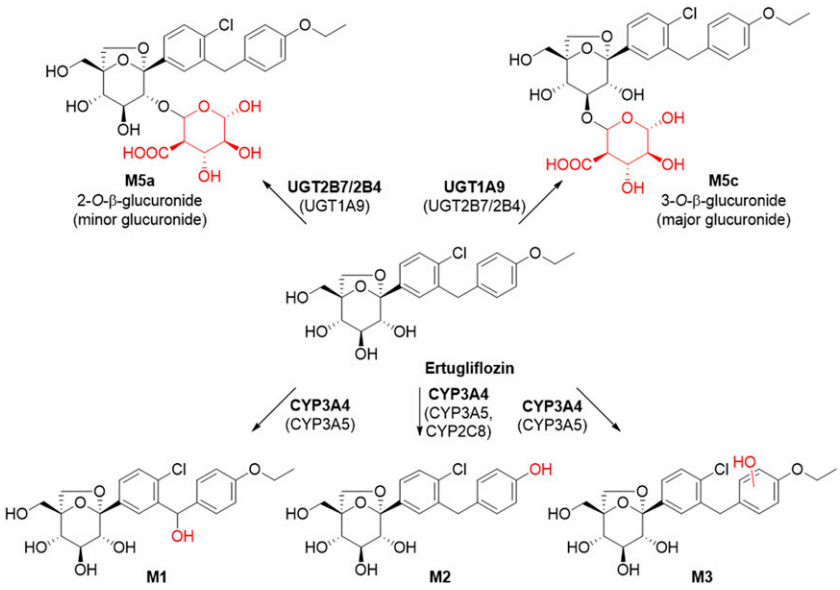

Fig. 1. Ertugliflozin human relevant metabolites identified from a mass-balance study.

glucose levels decreased and placebo-adjusted glycated hemoglobin levels decreased 0.99% and 1.16%, respectively (Terra et al., 2017). SGLT2 inhibitors demonstrated cardioprotective and renoprotective effects with treatment resulting in significant reductions in fasting plasma glucose, glycated hemoglobin, body weight, and blood pressure, as well as improved lipid profiles (Hollander et al., 2019; Tentolouris et al., 2019).

Absorption of ertugliflozin is rapid and complete with oral exposure increasing in a dose-proportional manner from 0.5 to 300 mg and an absolute oral bioavailability of ~100% (Raje et al., 2018). The absorption, distribution, metabolism, and excretion (ADME) of ertugliflozin was determined after a single oral dose of 25-mg [^{14}C] ertugliflozin (100 μCi) to healthy male subjects, and structures of key metabolites identified are presented in Fig. 1 (Miao et al., 2013). The primary clearance mechanism is metabolism with metabolite profiling in excreta indicating that the major route is glucuronidation with a minor contribution from oxidative metabolism. The major metabolite eliminated in human urine was ertugliflozin-3-*O*-*β*-glucuronide (M5c, previously M4c) (Miao et al., 2013), and a minor glucuronide was identified as ertugliflozin-2-*O*-*β*-glucuronide (M5a) (Fig. 1). Oxidative metabolism was minor with monohydroxylated ertugliflozin (M1 and M3) and des-ethyl ertugliflozin (M2) present in urine and feces. Ertugliflozin is completely absorbed (fraction absorbed of 111%) (Raje et al., 2018) with unchanged parent drug excreted in feces (~40%) presumably the result of glucuronide metabolite(s) that are excreted in the bile, hydrolyzed back to the parent drug in the intestine, and eliminated via the feces. Renal excretion of unchanged ertugliflozin was low (<2% of dose). Overall, the contribution of glucuronidation (86%), oxidative metabolism (12%), and renal excretion (2%) to ertugliflozin systemic clearance was based on the scaling of the human ADME study findings (Supplemental Table 1).

Preliminary reaction phenotyping or recombinant enzyme mapping indicated that UDP-glucuronosyltransferases (UGTs) 1A9 and 2B7 were able to catalyze ertugliflozin glucuronidation, and oxidative metabolism involved CYP3A4 (Kalgutkar et al., 2011). Since oxidative metabolism is a minor clearance (CL) pathway, clinically significant drug-drug interactions are not expected after coadministration with cytochrome P450 (CYP) inhibitors. Detailed quantitative UGT reaction phenotyping is required to predict the clinical drug-drug interaction risk when ertugliflozin is coadministered with UGT inhibitors. The objective of this study was to characterize the enzymes involved in the metabolism of ertugliflozin using in vitro human matrices. Reaction phenotyping for UGT and CYP enzymes was conducted using enzyme kinetics, recombinant enzyme systems, and isoform-selective chemical inhibitors.

Materials and Methods

Materials

Ertugliflozin or (1S,2S,3S,4R,5S)-5-[4-chloro-3-(4-ethoxybenzyl)phenyl]-1-hydroxymethyl-6,8-dioxabicyclo[3.2.1]octane-2,3,4-triol, M1 and M3, M2, M5c, M5a, and 16*β*-phenyllongifolol were obtained from Pfizer Global Research and Development Chemistry. Alamethicin, UDP glucuronic acid (UDPGA), $MgCl_2$, NADPH, diclofenac, terfenadine, furafylline, 2-phenyl-2-(1-piperdinyl)propane (PPP), montelukast, sulfaphenazole, benzylnirvanol, quinidine, ketoconazole, CYP3cide, tranilast, digoxin, 1 M potassium phosphate dibasic solution, 1 M potassium phosphate monobasic solution, Tris, bovine serum albumin (BSA; crude BSA product no. A7906), and DMSO were purchased from Sigma Aldrich (St. Louis, MO). Pooled human liver microsomes (HLMs) prepared from 50 mixed-gender donors and recombinantly expressed human UGT enzymes

ABBREVIATIONS: ADME, absorption, distribution, metabolism, and excretion; BSA, bovine serum albumin; CL, clearance; CL_{int}, apparent intrinsic clearance; $CL_{int,sc,u}$, scaled in vivo whole organ unbound intrinsic clearance; $CL_{int,u}$, unbound in vitro intrinsic clearance; f_{CL}, fraction of clearance; f_m, fraction of metabolism; f_u, fraction unbound; HKM, human kidney microsome; HLM, human liver microsome; IS, internal standard; ISEF, intersystem extrapolation factor; K_m, apparent substrate concentration at half-maximal velocity; K_{si}, inhibition constant for substrates exhibiting substrate inhibition kinetics; LC-MS/MS, liquid chromatography–tandem mass spectrometry; M1, monohydroxylated ertugliflozin; M2, des-ethyl ertugliflozin; M3, monohydroxylated ertugliflozin; M5a, 2-*O*-*β*-glucuronide; M5c, 3-*O*-*β*-glucuronide; CYP, cytochrome P450; PPP, 2-phenyl-2-(1-piperdinyl)propane; RAF, relative activity factor; $rhCL_{int}$, unbound intrinsic apparent clearance in rhUGTs; rhP450, recombinantly expressed human P450 enzymes; rhUGT, recombinantly expressed human UGT enzymes; S_{50}, substrate concentration at half-maximal velocity for substrates exhibiting atypical kinetics; SGLT, sodium-dependent glucose cotransporter; T2DM, type 2 diabetes mellitus; UDPGA, UDP glucuronic acid; UGT, UDP-glucuronosyltransferase; V_{max}, maximal rate of metabolism.

TABLE 1

Enzyme kinetic parameters for ertugliflozin glucuronide metabolite (M5a and M5c) formation in pooled HLMs

Data are expressed as the means ± S.D. from triplicate experiments, except M5c formation with 2% BSA (n = 6).

Incubation conditions[a]	K_m μM	$K_{m,u}$[b] μM	V_{max} pmol·min^{-1}·mg^{-1}	K_{si} μM	$CL_{int,u}$ μl·min^{-1}·mg^{-1}	$CL_{int,sc,u}$ ml·min^{-1}·kg^{-1}	$f_{CL,UGT}$
HLMs with 2% BSA							
M5a	379 ± 11	41.7	94.9 ± 1.2	—	2.28	2.15	0.06
M5c	98.3 ± 6.1	10.8	375 ± 7	—	34.7	32.8	0.94
Total	—	—	—	—	37.0	35.0	1.00
HLMs without BSA							
M5a[c]	3130 ± 1620	1690	734 ± 363	86.8 ± 46.8	0.434	0.410	0.05
M5c	77.5 ± 3.1	41.9	384 ± 4	—	9.16	8.66	0.95
Total	—	—	—	—	9.59	9.07	1.00

[a]HLM incubations were conducted in the presence and absence of 2% BSA as described under *Materials and Methods*.
[b]Ertugliflozin unbound fraction ($f_{u,inc}$) in HLMs (0.25 mg/ml) without BSA and with 2% BSA was 0.54 and 0.11, respectively.
[c]Apparent K_m values exceeded the highest ertugliflozin concentration in incubation (1000 μM) due to substrate inhibition kinetics.

(rhUGTs) (1A1, 1A3, 1A4, 1A6, 1A7, 1A8, 1A9, 1A10, 2B4, 2B7, 2B15, 2B17, and nontransfected control) were obtained from Corning Life Sciences (Woburn, MA). Pooled human kidney microsomes (HKMs) prepared from eight mixed-gender donors were obtained from Xenotech (Kansas City, KS). HLM 3A5*1*1, HLM 3A5*3/*3 microsomes pools were prepared as previously described (Tseng et al., 2014). Recombinantly expressed human CYPs (1A2, 2B6, 2C8, 2C9, 2C19, 2D6, 3A4, and 3A5) were obtained from either Invitrogen (Life Technologies, Waltham, MA) or BD BioSciences (Franklin Lakes, NJ).

General UGT Incubation Conditions

UGT incubations were performed in a buffer mixture containing 100 mM Tris HCl buffer (pH 7.5 at 37°C) with or without 2% BSA, 5 mM $MgCl_2$, and microsomal or recombinant protein. The buffer mixture was preincubated with alamethicin (10 μg/ml) on ice for 15 minutes to allow for alamethicin pore formation. The incubation mixture was warmed to 37°C prior to the addition of ertugliflozin. Reactions were initiated by the addition of 5 mM UDPGA and terminated by protein precipitation with acetonitrile containing internal standard (IS).

UGT Substrate Saturation in HLMs and rhUGTs

Using the general UGT incubation conditions described above, reactions with 0.25 mg/ml protein (i.e., HLM, rhUGT1A9, and rhUGT2B7) and ertugliflozin (1–1000 μM for HLMs, 0.33–1000 μM for rhUGTs) were initiated by the addition of UDPGA and terminated at 30 or 40 minutes by protein precipitation with acetonitrile containing IS. All samples were analyzed by liquid chromatography–tandem mass spectrometry (LC-MS/MS), where M5c and M5a formation were quantified against standard curves. The experimental conditions selected for enzyme kinetics were chosen after conduct of preliminary reaction rate experiments to ensure linear reaction velocity with respect to protein concentration and incubation time. HLM and rhUGT incubations for M5a formation were performed in triplicate. Incubations for M5c formation were conducted on several days (n = 6) in both HLMs and rhUGTs.

UGT Phenotyping

Ertugliflozin was incubated in the presence of 13 rhUGTs (1A1, 1A3, 1A4, 1A6, 1A7, 1A8, 1A9, 1A10, 2B4, 2B7, 2B10, 2B15, and 2B17) and nontransfected control to assess which isoforms contribute to glucuronide formation. The general incubation mixture without 2% BSA contained 0.5 mg/ml protein, either rhUGT or vector control, and ertugliflozin (7, 77, and 770 μM) representing approximately 0.1×, 1×, and 10× the HLM apparent substrate concentration at half-maximal velocity (K_m) for the primary glucuronidation (M5c) pathway (Table 1). The incubation mixtures were prewarmed to 37°C prior to the addition of UDPGA and terminated over a time course by protein precipitation with acetonitrile containing IS. Samples were analyzed by LC-MS/MS, where ertugliflozin depletion and both M5c and M5a formation were measured by analyte/IS area ratios. All incubations were performed in duplicate.

Ertugliflozin (5 μM) was incubated with HLMs in the presence of 2% BSA with and without UGT chemical inhibitors for a quantitative assessment of UGT isoform contribution. General incubation conditions and sample preparation were similar to those described for UGT substrate saturation experiments. Reversible inhibitors were incubated at the following concentrations: 10 μM tranilast (UGT1A9), 10 μM digoxin (UGT1A9), and 3 μM 16β-phenyllongifolol (UGTs 2B4/2B7). Control incubations were performed in the absence of chemical inhibitors (HLM control). The incubation mixture was warmed to 37°C for 5 minutes prior to the addition of ertugliflozin. Reactions were initiated by the addition of UDPGA and terminated over a time course by protein precipitation with acetonitrile containing IS. Samples were analyzed using LC-MS/MS, where M5a and M5c formation were quantified against standard curves. Selective chemical inhibition experiments were conducted in duplicate.

CYP Substrate Saturation in HLMs and Recombinantly Expressed Human CYP Enzymes

HLM incubation mixtures contained 100 mM potassium phosphate buffer (pH 7.4), 3 mM $MgCl_2$, 0.1 mg/ml HLMs, and ertugliflozin (0.01–1000 μM). Incubations were warmed to 37°C prior to the addition NADPH (1.2 mM). Reactions were terminated after 10 minutes by transferring aliquots of the incubation mixture to acetonitrile containing IS. Incubations were conducted in duplicate. For substrate saturation experiments in recombinantly expressed human CYP enzymes (rhP450s) (2C8, 3A4, and 3A5), incubation conditions were similar to those described previously in HLMs. The rhP450 concentration was 10 pmol/ml (0.11 mg/ml) protein, the incubation time was 10 minutes, and ertugliflozin concentrations ranged from 0.01 to 500 μM. All samples were analyzed by LC-MS/MS and quantified against standard curves of M1, M2, and M3. The experimental conditions selected for enzyme kinetics were chosen after conduct of preliminary reaction rate experiments in HLMs to ensure linear reaction velocity with respect to protein concentration and incubation time.

CYP Phenotyping

Ertugliflozin was incubated in the presence of eight rhP450 (1A2, 2B6, 2C8, 2C9, 2C19, 2D6, 3A4, and 3A5) at a concentration of 10 pmol/ml. Potassium phosphate buffer (100 mM), rhP450s or nontransfected control, and ertugliflozin (10 μM for M1 and M2 formation, or 50 μM for M3 formation) were prewarmed to 37°C. Incubations were initiated with 1.2 mM NADPH followed by addition of substrate. Reactions were terminated at 10 minutes by protein precipitation with acetonitrile containing IS. The recombinant CYP panel was incubated in triplicate. All samples were analyzed by LC-MS/MS and quantified against standard curves of M1, M2, and M3.

Ertugliflozin (10 or 50 μM) was incubated with HLMs in the presence of CYP selective chemical inhibitors for the determination of CYP isoform contribution. General incubation conditions and sample preparation were similar to those described for CYP substrate saturation experiments. Reversible inhibitors were incubated at the following concentrations: 0.64 μM montelukast (CYP2C8), 10 μM sulfaphenazole (CYP2C9), 3 μM benzylnirvanol (CYP2C19), 1 μM quinidine (CYP2D6), and 1 μM ketoconazole (CYP3A4/5). Inactivators were preincubated at the following concentrations: 10 μM furafylline (CYP1A2), and 3 μM PPP (CYP2B6). For incubations containing reversible inhibitors, microsomes were preincubated with inhibitors for 5 minutes prior to initiating the

reactions by the addition of NADPH or buffer minus NADPH control followed immediately by ertugliflozin. Incubations containing the inactivator furafylline or PPP were preincubated with NADPH and microsomes for 20 minutes to achieve complete inactivation of the respective CYP isoform prior to the addition of ertugliflozin. Control incubations were performed in the absence of chemical inhibitors (HLM control). Selective chemical inhibition experiments were conducted in triplicate. All samples were analyzed by LC-MS/MS and quantified against standard curves of M1, M2, and M3.

To discern the relative contributions of CYPs 3A4 and 3A5 to the metabolism of ertugliflozin, additional experiments were conducted in a pooled lot of HLMs prepared from individual HLM lots selected for either the *1/*1 genotype (HLM 3A5 *1/*1) associated with CYP3A5 extensive metabolizers or *3/*3 genotype (HLM 3A5 *3/*3) associated with CYP3A5 poor metabolizers (Tseng et al., 2014). Microsomal incubations with ertugliflozin (10 and 50 μM) were conducted as described above for HLMs (0.1 mg/ml protein, 10-minute incubation) and included 1 μM ketoconazole (CYP3A4/5 inhibitor) or 1 μM CYP3cide (CYP3A4 inhibitor). Pretreatment of the incubates varied based on the presence of the competitive inhibitor ketoconazole (no preincubation with NADPH) or the inactivator CYP3cide (10-minute preincubation with NADPH). The control incubation for these experiments was conducted with no preincubation. These experiments were conducted in duplicate. All samples were analyzed by LC-MS/MS and quantified against standard curves of M1, M2, and M3.

Ertugliflozin Clearance in HLMs and HKMs by Substrate Depletion

The clearance of ertugliflozin was investigated in HLMs and HKMs in the presence of the individual and combined cofactors (e.g., UDPGA and/or NADPH) to estimate the in vitro fraction of metabolic clearance (f_{CL}) by UGT or CYP enzyme families. Incubations were performed using the general UGT incubation conditions described above with and without 2% BSA containing 2 mg/ml HLMs or HKMs. The incubation mixture was warmed to 37°C prior to the addition of UDPGA (5 mM) or NADPH (1.6 mM), either as a mixture or individually. Reactions were initiated by the addition of ertugliflozin (1 μM final) and terminated over a time course from 0 to 180 minutes by protein precipitation with acetonitrile containing IS. All incubations were performed in duplicate. Samples were analyzed by LC-MS/MS and quantified against standard curves of ertugliflozin, M5c, and M5a.

Determination of Unbound Fraction of Ertugliflozin in HLMs

Using the equilibrium dialysis method previously described (Di et al., 2012), the fraction unbound (f_u) in HLMs was determined using 1 μM ertugliflozin. For UGT HLM incubation conditions, binding was determined with and without 2% BSA at a protein concentration of 0.25 mg/ml HLMs. Additional components of the donor chamber mimicked the incubation mixture described in *Materials and Methods* on *UGT Substrate Saturation in HLMs and rhUGTs*, except that UDPGA was omitted. The receiver chamber contained Tris buffer containing 5 mM $MgCl_2$. For binding under CYP incubation conditions, f_u was determined in the incubation components described in *Materials and Methods* on *CYP Substrate Saturation in HLMs and Recombinantly Expressed Human CYP Enzymes*, except that NADPH was omitted and the protein concentration was 0.76 mg/ml HLM. Samples were placed in a CO_2 incubator (5% CO_2, 75% relative humidity) for 6 hours at 37°C. Ertugliflozin recovery, stability, and binding samples were matrix matched and protein precipitated with acetonitrile containing IS. Samples were analyzed for ertugliflozin and the IS by LC-MS/MS. Peak area ratio of analyte/internal standard was used to calculate f_u, recovery, and stability.

Data Analysis

Clearance by Substrate Depletion. The unbound in vitro intrinsic clearance ($CL_{int,u}$) and scaled in vivo whole organ intrinsic clearance ($CL_{int,sc,u}$) was determined at a single ertugliflozin concentration and determined by depletion using the following equations:

$$t^{1/2} = \frac{0.693}{k_{el}} \tag{1}$$

$$CL_{int,u} = \left(\frac{0.693}{t\$} \times \frac{mlincubation}{mgprotein} \times \frac{1000\mu l}{ml}\right)/f_u \tag{2}$$

$$CL_{int,sc,u} = \left(\frac{0.693}{t^{1/2}} \times \frac{mlincubation}{microsomes} \times \frac{Xmgmicrosomes}{goftissue} \times \frac{Ygoftissue}{kgofbodyweight}\right)/f_u \tag{3}$$

where the elimination rate constant (k_{el}) is negative slope of natural log of the average peak area ratio versus time, and f_u is the fraction unbound in the incubation ($f_{u,inc}$). For HLMs, X and Y were 45 and 21, respectively. For HKMs, X and Y were 12.8 and 4.5, respectively. The $CL_{int,u}$ was also determined by metabolite formation at a single ertugliflozin concentration using the equation

$$CL_{int,u} = \left(formation\ rate \frac{pmol}{ml \times min} \times \frac{mL\ incubation}{mg\ microsomes} \times \frac{1000\ \mu l}{ml} \times \frac{ml\ incubation}{pmol\ substrate}\right)/f_u \tag{4}$$

where formation rate is the slope of metabolite formation. Using eq. 3, the $CL_{int,sc,u}$ was calculated and used to estimate systemic clearance for the relevant metabolic organ. The f_{CL} for renal metabolism was calculated using eq. 5:

$$f_{CL}\ renal = \frac{CL_{int,sc,u,renal}}{CL_{int,sc,u,renal} + CL_{int,sc,u,hepatic}} \tag{5}$$

Clearance in HLMs Using Enzyme Kinetic Parameters. In general, substrate concentration [S] and velocity (v) data were fit to the appropriate enzyme kinetic model by nonlinear least-squares regression analysis to derive the apparent enzyme kinetic parameters, maximal rate of metabolism (V_{max}), and K_m or S_{50}. The Michaelis-Menten model (eq. 6), the substrate activation model (eq. 7) which incorporates the Hill coefficient (n), and the substrate inhibition model (eq. 8) were evaluated for best fit of the data. Best fit was determined using R^2 goodness of fit, Eadie-Hofstee fit, and Akaike information criterion.

$$v = \frac{V_{max} \times S}{(K_m + S)} \tag{6}$$

$$v = \frac{V_{max} \times S^n}{(S_{50}^n + S^n)} \tag{7}$$

$$v = \frac{V_{max} \times S}{K_m + S \times \left(1 + \frac{S}{K_i}\right)} \tag{8}$$

The exception was formation of M1 in rhCYP2C8. An unweighted linear fit was used the calculate the formation slope [i.e., apparent intrinsic clearance (CL_{int})] since M1 formation was not saturable (Supplemental Fig. 3) with the highest concentration of ertugliflozin in incubation (500 μM). The $CL_{int,u}$ was calculated using either eq. 9 for typical kinetics or for M1 formation in rhCYP2C8, CL_{int} was equivalent to the linear slope. Equation 10 was used to calculate $CL_{int,u}$ atypical kinetics incorporating the Hill coefficient.

$$CL_{int,u} = \left(\frac{V_{max}}{K_m}\right)/f_u \tag{9}$$

$$CL_{int,u} = \left(\frac{V_{max}}{S_{50}} \times \frac{(n-1)}{n \times (n-1)^{1/n}}\right)/f_u \tag{10}$$

The contribution of each metabolic pathway (as represented by each metabolite) to the total clearance of ertugliflozin (f_{CL}) was calculated using eq. 11:

$$f_{CL} = \frac{CL_{int,u,x}}{\sum CL_{int,tot,u}} \tag{11}$$

where $CL_{int,u,x}$ is the unbound apparent intrinsic clearance for metabolite x, and $CL_{int,tot,u}$ is the sum of unbound scaled intrinsic apparent clearance values for all metabolites measured.

Fraction of Metabolism Using Selective Chemical Inhibitors in HLMs. The effect of selective chemical inhibitors on the formation of each metabolite was calculated using eq. 12:

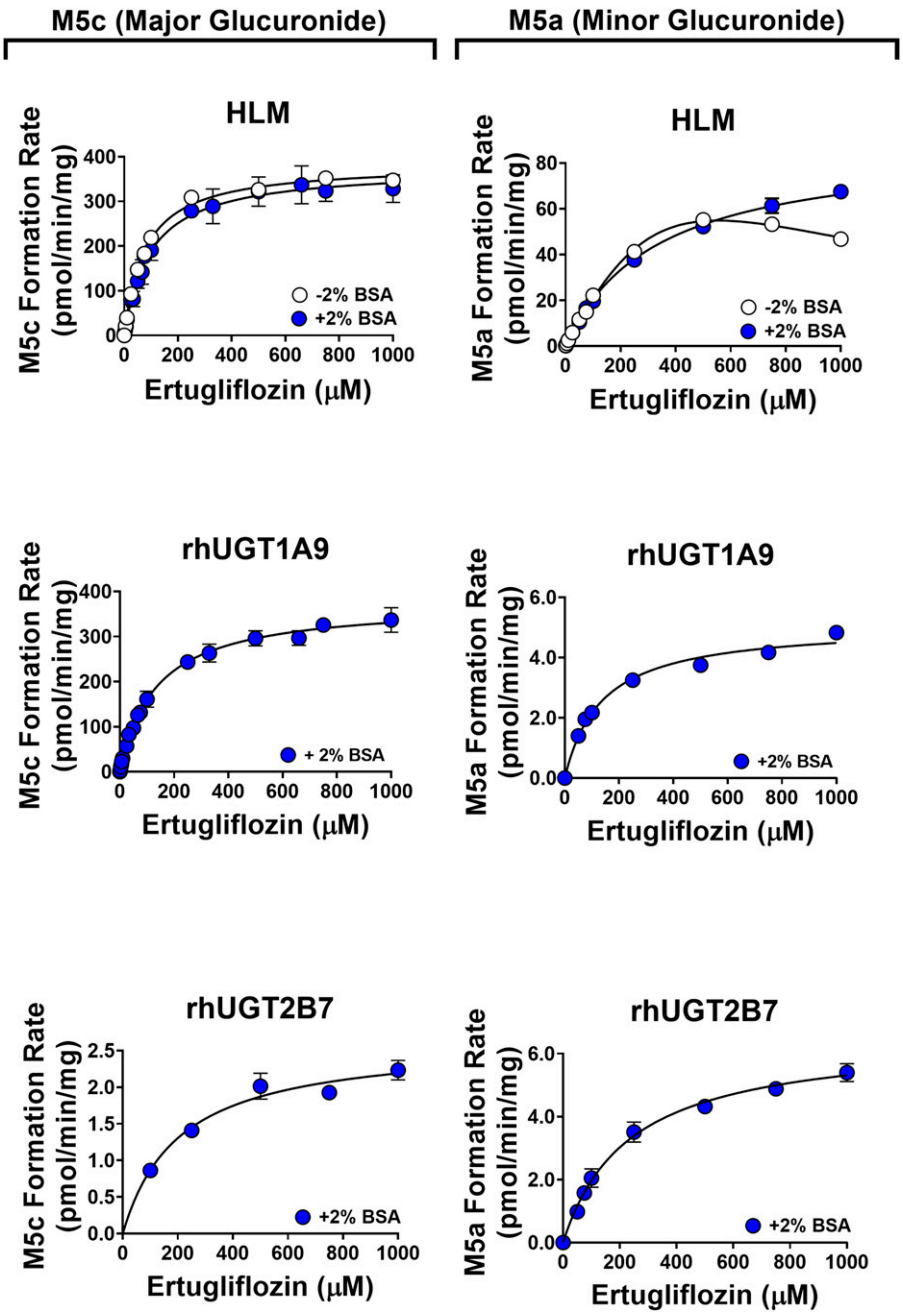

Fig. 2. Substrate saturation profiles of ertugliflozin glucuronide metabolites, M5c and M5a, derived from pooled HLMs, rhUGT1A9, and rhUGT2B7. HLM data were generated in the absence (open circles) and presence of 2% BSA (blue circles), whereas rhUGT kinetics were conducted in the presence of 2% BSA as described under *Materials and Methods*. Data are expressed as the means ± S.D. from triplicate experiments, except M5c formation with 2% BSA (n = 6).

$$\%Inhibition = \left(1 - \frac{Inhibitor\ CL_{int,u}}{No\ Inhibitor\ CL_{int,u}}\right) \times 100 \quad (12)$$

To determine the isoform specific contribution to total clearance, metabolite specific contributions were adjusted for fractional clearance:

$$f_m = Inhibition_x \times f_{m,CL_{tot,u,x}} \quad (13)$$

where $Inhibition_x$ is the contribution of a specific isoform to the formation of metabolite x, and $f_{m,CLtot,u,x}$ is the fraction of total clearance represented by metabolite x. Since two inhibitors were used for UGT1A9, the mean % inhibition was used for the final fraction of metabolism (f_m) estimate.

Using Relative Activity Factor or Intersystem Extrapolation Factor to Scale Recombinantly Expressed Enzyme Clearance to HLM Clearance. The rhUGT 1A9 and 2B7 $CL_{int,u}$ was calculated using eq. 9, which was then scaled to HLM $CL_{int,u}$ using eq. 14:

$$HLM\ CL_{int,u} = RAF \times rhCL_{int,u} \quad (14)$$

where RAF is the relative activity factor for an individual enzyme based on selective probe substrate CL_{int} values (eq. 15), $rhCL_{int}$ is the unbound intrinsic apparent clearance in rhUGTs, and CL_{int} is the unbound intrinsic apparent clearance scaled to liver. The RAF value for UGT1A9 (0.8) was generated using mycophenolic acid as the substrate. The UGT2B7 RAF value of 2.4 was generated using zidovudine.

$$RAF = \frac{HLMCL_{int}}{rhCL_{int}} \quad (15)$$

For rhCYP 3A4, 3A5, and 2C8 incubations, the $rhCL_{int,u}$ was calculated (eq. 9). An intersystem extrapolation factor (ISEF) was applied in conjunction with the abundance of the CYP in the liver (Supplemental Table 2) to scale to a hepatic $CL_{int,u}$.

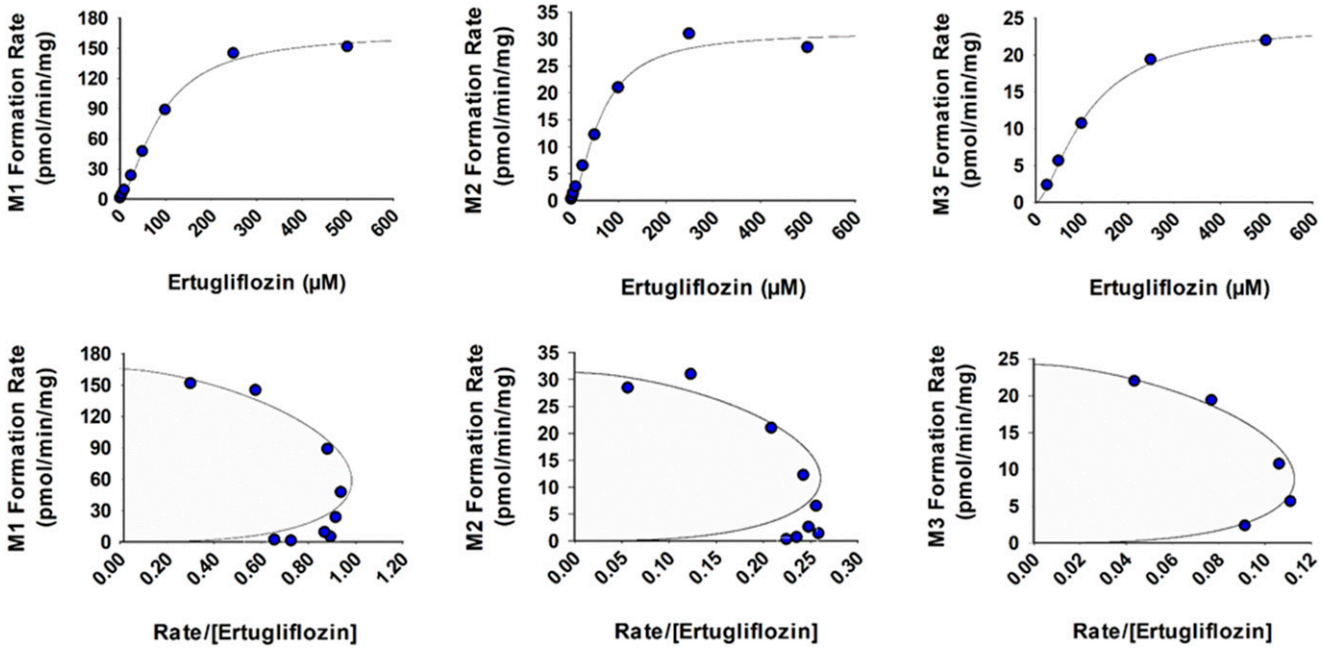

Fig. 3. Substate saturation profile of ertugliflozin oxidative metabolites M1, M2, and M3 derived from pooled HLMs. The kinetic profiles exhibited a sigmoidal behavior, as illustrated by the Eadie-Hofstee graphs. Data are expressed as the means from duplicate experiments.

$$HLM\ CL_{int,u} = rhCL_{int,u} \times ISEF \times tissue\ abundance \frac{pmol}{mg} \quad (16)$$

Delineation of the Fraction Metabolized via CYP3A4 versus CYP3A5. The linear portion of the mean regression line (n = 2) was used to determine a single slope of each incubation condition (k_{el}). The slope of the line was used to determine the half-life ($t_{1/2}$; minutes) at each incubation condition (eq. 1), which was then extrapolated to the CL_{int}, like eq. 2. The contribution by CYP3A5 was calculated using the following equations (Tseng et al., 2014):

$$Calculated\ \%\ CYP3A4\ Contribution = \frac{CL_{int,cnt} - CL_{int,CYP3cide}}{CL_{int,cnt}} \times 100 \quad (17)$$

$$Calculated\ \ \%CYP3A5\ Contribution = \%CYP3A - \%CYP3A4 \quad (18)$$

where $CL_{int,cnt}$ is the clearance in HLMs without inhibitor.

Results

UGT and CYP Substrate Saturation in HLMs. The metabolite formation kinetics for ertugliflozin glucuronides M5c (major) and M5a (minor) were determined after incubation of ertugliflozin in HLMs in the absence and presence of 2% BSA (Fig. 2; Table 1). In the absence of BSA, M5a exhibited substrate inhibition kinetics, and the estimated apparent K_m value (3130 μM) exceeded the highest ertugliflozin concentration in incubation (1000 μM). All other profiles displayed typical Michaelis-Menten kinetics. In general, the $K_{m,u}$ values were lower in the presence of 2% BSA for M5c (4-fold) and M5a (41-fold) resulting in $K_{m,u}$ values of 10.8 and 41.7 μM, respectively. Inclusion of BSA had minimal effect on M5c V_{max}, whereas M5a V_{max} decreased in the presence of BSA from 734 ± 363 to 94.9 ± 1.2 pmol/min per milligram. Overall, the formation $CL_{int,u}$ for M5c and M5a increased >3.8-fold in the presence of BSA primarily driven by a lower $K_{m,u}$. The highest total $CL_{int,u}$ for glucuronidation (37 μl/min per milligram) was observed in the presence of BSA with M5c (34.7 μl/min per milligram) the primary and M5a (2.28 μl/min per milligram) the minor metabolic route.

CYP enzyme kinetic and intrinsic clearance values were determined for the formation of M1, M2, and M3 in HLMs (Fig. 3; Table 2). Visual inspection of the Eadie-Hofstee plots for the M1, M2, and M3 reaction rates demonstrated nonlinear profiles consistent with activation kinetics. For all three metabolites, a Michaelis-Menten equation including a Hill coefficient best described the formation kinetics and was selected for determination of enzyme kinetic parameters. $S_{50,u}$, V_{max}, and Hill coefficient values were 73.0 μM, 166 pmol/min per milligram, and 1.54 for M1, 51.6 μM, 31.4 pmol/min per milligram, and 1.59 for M2, and 93.0 μM, 24.3 pmol/min per milligram, and 1.56 for M3, respectively.

TABLE 2

Enzyme kinetic parameters for ertugliflozin oxidative metabolite (M1, M2, and M3) formation in pooled HLMs

Data are expressed as the means from duplicate experiments after HLM incubations as described under Materials and Methods.

HLM metabolite	S_{50}	$S_{50,u}$[a]	V_{max}	Hill coefficient	$CL_{int,u}$	$CL_{int,sc,u}$	$f_{CL,CYP}$
	μM	μM	pmol·min^{-1}·mg^{-1}		μl·min^{-1}·mg^{-1}	ml·min^{-1}·kg^{-1}	
M1	88.0	73.0	166	1.54	1.19	1.12	0.72 (0.73)[b]
M2	62.2	51.6	31.4	1.59	0.315	0.297	0.19
M3	112	93.0	24.3	1.56	0.136	0.129	0.083 (0.084)[b]
Total	—	—	—	—	1.64	1.55	0.99 (1.0)[b]

[a]Ertugliflozin unbound fraction ($f_{u,inc}$) was calculated as 0.83 for 0.1 mg/ml protein in incubation based on the measured value of 0.397 at 0.76 mg/ml HLMs.
[b]Values in parenthesis are the fractional clearances normalized to a value of 1.0.

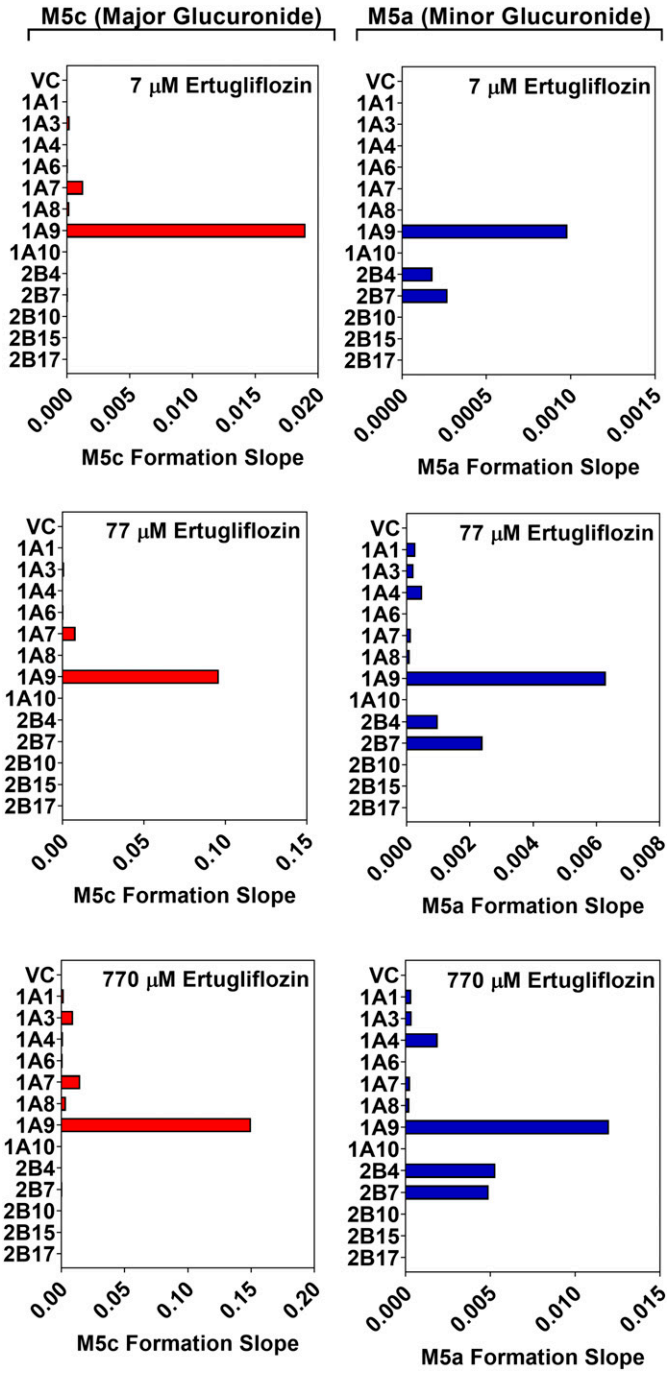

Fig. 4. Formation of ertugliflozin glucuronide metabolites M5c and M5a incubated with 13 rhUGT enzymes in the absence of 2% BSA. Ertugliflozin was incubated at concentrations of 7, 77, and 770 μM representing 0.01×, 1× and 10× the M5c (Table 1). Data are expressed as the means from duplicate experiments.

Based on these kinetic parameters, the respective M1, M2, and M3 $CL_{int,sc,u}$ values were 1.12, 0.297, and 0.129 ml/min per kilogram.

The overall UGT-mediated $CL_{int,sc,u}$ in the presence of BSA was 35.0 ml/min per kilogram, whereas the overall CYP mediated $CL_{int,sc,u}$ for ertugliflozin was 1.55 ml/min per kilogram. With a combined UGT- and CYP mediated $CL_{int,sc,u}$ of 36.4 ml/min per kilogram, the in vitro f_m for UGT- and CYP mediated metabolism was 0.96 and 0.04, respectively (Fig. 6). Using the UGT-mediated $CL_{int,sc,u}$ without 2% BSA (9.07 ml/min per kilogram), the combined UGT- and CYP mediated $CL_{int,sc,u}$ decreased to 10.6 ml/min per kilogram.

UGT Phenotyping of Ertugliflozin. UGT phenotyping or enzyme mapping with rhUGTs (UGT1A1, 1A3, 1A4, 1A6, 1A7, 1A8, 1A9, 1A10, 2B4, 2B7, 2B10, 2B15, and 2B17) was conducted after incubation of ertugliflozin with rhUGTs in the absence of BSA to investigate formation of M5c and M5a at ertugliflozin concentrations approximately 0.1×, 1× and 10× the primary glucuronide (M5c) HLM K_m (7, 77, and 770 μM ertugliflozin) (Fig. 4; Supplemental Table 3). At low substrate concentrations (7 μM ertugliflozin), four UGTs (1A9, 1A3, 1A7, and 1A8) were able to catalyze formation of the major glucuronide (M5c) with UGT1A9 as the apparent dominant isoform. At higher ertugliflozin concentrations, M5c was quantifiable in other UGT1A enzyme incubations (i.e., 1A1, 1A3, 1A4, 1A6, 1A7, 1A8) and UGTs 2B7, 2B15 and 2B17, albeit trace or minor relative to UGT1A9. The minor glucuronide (M5a) formation as was quantifiable with UGTs 1A9, 2B7, and 2B4 at low substrate concentration and relative product formation increased at higher substrate concentrations with metabolic turnover observed for UGTs 1A4, 1A1, 1A3, 1A7, and 1A8.

To provide a quantitative assessment of the contribution of the apparently major UGTs 1A9, 2B4, and 2B7 observed in UGT enzyme mapping (Fig. 4) toward M5c and M5a formation, the effects of chemical inhibitors on the metabolism of ertugliflozin in HLMs were investigated (Supplemental Fig. 1; Table 3). Formation of M5c was inhibited 88.0% by tranilast (UGT1A9), 81.8% by digoxin (UGT1A9), and 13.9% by 16β-phenyllongifolol (UGT2B4/2B7). The inhibition results were scaled to 100% to achieve a mean f_m UGT1A9 and UGT2B4/2B7 of 0.86 and 0.14, respectively, for formation of the major in vitro glucuronide. For M5a, mean UGT1A9 inhibition and UGT2B4/2B7 inhibition resulted in f_m values of 0.20 and 0.80, respectively. The combined inhibition of overall in vitro glucuronidation in HLMs resulted in a f_m for UGT1A9 and UGT2B4/2B7 of 0.81 and 0.19, respectively.

Enzyme kinetic characterization describing formation of M5c and M5a in rhUGT 1A9 and 2B7 were performed in the presence of 2% BSA (Fig. 2; Table 4). All profiles exhibited typical Michaelis-Menten kinetics. For M5c, the $K_{m,u}$ and V_{max} in rhUGTs 1A9 and 2B7 was 14.7 μM and 375 ± 5 pmol/min per milligram ($rhCL_{int,u}$ = 25.4 μl/min per milligram), and 22.4 μM and 2.63 ± 0.18 pmol/min per milligram ($rhCL_{int,u}$ = 0.177 μl/min per milligram), respectively. For M5a, the $K_{m,u}$ and V_{max} in rhUGTs 1A9 and 2B7 were 14.9 μM and 5.09 ± 0.15 pmol/min per milligram ($rhCL_{int,u}$ = 0.343 μl/min per milligram), and 25.6 μM and 6.55 ± 0.28 pmol/min per milligram ($rhCL_{int,u}$ = 0.256 μl/min per milligram), respectively. The $rhCL_{int,u}$ was scaled to hepatic $CL_{int,u}$ using the appropriate RAF (Table 4). For UGT1A9, a mycophenolic acid generated RAF of 0.8 (Lin et al., 2015) was used to scale M5c and M5a formation to a hepatic microsomal $CL_{int,u}$ of 20.4 and 0.274 μl/min per milligram, respectively. Zidovudine was used to generate a UGT2B7 RAF of 2.4 (Lin et al., 2014). UGT2B7 mediated hepatic $CL_{int,u}$ for M5c and M5a formation was 2.81 and 0.613 μl/min per milligram, respectively. Overall, addition (M5c and M5a) of the RAF-adjusted scaled HLM CL_{int} for UGT1A9 (20.7 μl/min per milligram) and UGT2B7 (3.42 μl/min per milligram) results in the combined UGT-mediated $CL_{int,u}$ of 24.1 μl/min per milligram ($CL_{int,sc,u}$ = 22.7 ml/min per kilogram) or RAF-adjusted f_m UGT1A9 and UGT2B7 of 0.86 and 0.14, respectively. (The rhUGT CL_{int} prior to RAF scaling yields f_m UGT1A9 and UGT2B7 of 0.986 and 0.014, respectively).

CYP Phenotyping of Ertugliflozin. CYP reaction phenotyping or enzyme mapping was conducted examining ertugliflozin metabolite formation in eight rhP450s (CYP1A2, 2B6, 2C8, 2C9, 2C19, 2D6, 3A4, and 3A5), which revealed M1 formation was quantifiable in rhCYPs 1A2, 3A4, and 3A5, M2 was quantifiable in rhCYPs 1A2, 2C8, 2C19, 2D6, 3A4, and 3A5, and M3 was quantifiable in rhCYPs 2D6, 3A4, and 3A5 (Supplemental Fig. 2).

TABLE 3

Inhibition of ertugliflozin (5 μM) glucuronide formation in pooled HLMs using UGT-selective chemical inhibitors

Data are expressed as the means from duplicate experiments after HLM incubations as described under Materials and Methods. The relative contribution values (f_m) were calculated from data scaled to 100% inhibition.

UGT enzyme	Inhibitor	Ertugliflozin metabolite formation								
		M5a			M5c			Total (M5a + M5c)		
		$CL_{int,u}$ [a] μl·min^{-1}·mg^{-1}	Inhibition (scaled to 100%) %	Relative contribution f_m	$CL_{int,u}$ [a] μl·min^{-1}·mg^{-1}	Inhibition (scaled to 100%) %	Relative contribution f_m	$CL_{int,u}$ [a] μl·min^{-1}·mg^{-1}	Inhibition (scaled to 100%) %	Relative contribution f_m
HLM	Control incubation	4.92	—	—	60.0	—	—	64.9	—	—
1A9	10 μM tranilast	3.91	20.6	—	7.18	88.0	—	11.7	82.0	—
1A9	10 μM digoxin	4.08	17.2	—	10.9	81.8	—	15.0	76.9	—
1A9	Mean digoxin/tranilast	3.99	18.9 (19.7)	0.20	9.04	84.9 (85.9)	0.86	13.0	80.0 (81)	0.81
2B4/2B7	3 μM 16β-phenyllongifolol	0.908	76.8 (80.3)	0.80	51.7	13.9 (14.1)	0.14	52.6	19.0 (19)	0.19

[a]Ertugliflozin unbound fraction ($f_{u,inc}$) in HLMs with 2% BSA was 0.11.

The effect of CYP selective chemical inhibitors on the metabolism of ertugliflozin in HLMs was also investigated. The metabolic formation rates of M1, M2 and M3 in HLMs were most significantly inhibited in the presence of ketoconazole resulting in percent inhibition values of 91.9%, 86.8%, and >81.8%, respectively (Table 5). After scaling inhibition responses to 100%, f_m for CYP3A4/5 was predicted to be 0.72 for M1, 0.15 for M2, and >0.080 for M3. M2 was also significantly inhibited in the presence of montelukast resulting in a percent inhibition value of 24.7% and a predicted f_m CYP2C8 of 0.042. Minor contributions by the remaining CYP isoform inhibitors were observed for M1 (2C8, 2C9, 2D6), M2 (1A2, 2B6, 2C9, 2D6), and M3 (2B6, 2C8, 2C9), although inhibition did not achieve statistical significance ($P > 0.01$) and was considered negligible.

To further discern the contribution of CYP isoforms 3A4 and 3A5 to ertugliflozin metabolism, incubations with the CYP3A4 selective inactivator CYP3cide and dual CYP3A4/5 inhibitor ketoconazole were conducted in CYP3A5 high (HLM 3A5 *1/*1) and low expressing (HLM 3A5 *3/*3) microsomes (Fig. 5; Supplemental Table 4). There were statistically significant differences ($P < 0.01$) in the percent inhibition of M1 and M2 resulting from incubation with CYP3cide (75% and 68%) when compared with ketoconazole (84% and 86%) indicating a contribution by CYP3A5 in metabolism of ertugliflozin, albeit small. The calculated in vitro contribution of CYP3A5 to overall CYP3A metabolism of M1 and M2 was 9.7% and 18%, respectively (Supplemental Table 4). In HLM 3A5 *1/*1, the percent inhibition of M3 by CYP3cide (81%) was not statistically different when compared with ketoconazole (88%). When incubated in microsomes devoid of CYP3A5 expression (HLM 3A5 *3/*3), there was no statistically meaningful difference between the effects of CYP3cide and ketoconazole on any of the metabolites.

Ertugliflozin kinetic parameters were generated for all three metabolites in rhCYP 3A4, 3A5, and 2C8 (Supplemental Fig. 3; Table 4). rhCYP3A4 kinetics was best described by the substrate inhibition model with $K_{m,u}$, V_{max}, and inhibition constant for substrates exhibiting substrate inhibition kinetics (K_{si}) values of 120 μM, 37.0 pmol/min per picomole and 1090 μM for M1, 135 μM, 11.0 pmol/min per picomole and 587 μM for M2, and 213 μM, 15.6 pmol/min per picomole and 397 μM for M3, respectively. Based on these kinetic parameters, the respective M1, M2, and M3 $CL_{int,sc,u}$ values were 4.78, 1.27, and 1.13 ml/min per kilogram (after ISEF and abundance scaling). rhCYP2C8 M2 metabolite formation was best fit to a substrate inhibition model for determination of enzyme kinetic parameters. K_m, V_{max}, and K_i values for M2 formation were 32.0 μM, 0.0361 pmol/min per picomole, and 568 μM. The resulting hepatic $CL_{int,sc,u}$ value for M2 was 0.0654 ml/min per kilogram. Kinetic parameters for M1 with rhCYP2C8 were not calculated due to insufficient solubility to achieve saturation V_{max}. A $CL_{int,sc,u}$ value for M1 of 0.0174 ml/min per kilogram was calculated from the slope of substrate concentration versus formation rate data. M3 formation with rhCYP2C8 was detectable but did not have sufficient measurable concentration data to generate a kinetic curve. The total scaled, ISEF-adjusted, $CL_{int,cs,u}$ for CYP2C8 contribution to ertugliflozin metabolism was 0.083 ml/min per kilogram. In rhCYP3A5, M1 and M2 reaction rates were fit to a substrate inhibition model, and M3 was fit to a Michaelis-Menten model for determination of enzyme kinetic parameters. $K_{m,u}$, V_{max}, and K_i values for M1 and M2 formation in rhCYP3A5 were 175 μM, 5.47 pmol/min per picomole, and 1660 μM and 163 μM, 4.93 pmol/min per picomole, and 771 μM, respectively. The $K_{m,u}$ and V_{max} values for M3 formation are 495 μM and 1.66 pmol/min per picomole. Based on these kinetic parameters, the respective M1, M2, and M3 rhP450 $CL_{int,u}$ values were 0.0313, 0.0302, and 0.0044 μl/min per picomole, respectively. HLM $CL_{int,u}$ values were not calculated due to lack of CYP3A5 ISEF. The total $CL_{int,sc,u}$ for CYPs was 7.26 ml/min

TABLE 4

Enzyme kinetic parameters for ertugliflozin metabolite formation in recombinantly expressed CYP and UGT enzymes

Data are expressed as the means ± S.D. from triplicate incubations or means from duplicate experiments. Recombinant enzyme kinetics were scaled to HLM CL_{int} using the HLM Scaling Factors (RAF for UGTs and ISEF for CYPs) as described under Materials and Methods.

Metabolite	Enzyme	V_{max}[a]	K_m	$K_{m,u}$	K_{si}	$rhCL_{int,u}$[b]	HLM scaling factor[c,d]	HLM $CL_{int,u}$[b]	HLM $CL_{int,sc,u}$[b]	Combined $CL_{int,sc,u}$	f_m by enzyme family[e]
			μM	μM	μM	$\mu l \cdot min^{-1} \cdot mg^{-1}$		$\mu l \cdot min^{-1} \cdot mg^{-1}$	$ml \cdot min^{-1} \cdot kg^{-1}$	$ml \cdot min^{-1} \cdot kg^{-1}$	
M5a	UGT1A9	5.09 ± 0.15	135 ± 13	14.9	—	0.343	0.80	0.274	0.259	22.7	UGT: 0.76 (1A9:2B7
	UGT2B7	6.55 ± 0.28	233 ± 28	25.6	—	0.256	2.40	0.613	0.580		0.86:0.14)
M5c	UGT1A9	375 ± 5	134 ± 6	14.7	—	25.4	0.80	20.4	19.2		
	UGT2B7	2.63 ± 0.18	204 ± 46	22.4	—	0.117	2.40	2.81	2.66		
M1	CYP3A4	37.0	148	120	1090	0.308	16.4	5.05	4.78	7.26	CYP: 0.24
	CYP3A5	5.47	230	175	1660	0.0313	—	—	—		
	CYP2C8[f]	—	—	—	—	0.0003	55.2	0.0184	0.0174		
M2	CYP3A4	11.0	167	135	587	0.0815	16.4	1.34	1.27		
	CYP3A5	4.93	215	163	771	0.0302	—	—	—		
	CYP2C8	0.0361	32.0	28.8	568	0.00125	55.2	0.0692	0.0654		
M3	CYP3A4	15.6	263	213	397	0.0732	16.4	1.20	1.13		
	CYP3A5	1.66	495	376	—	0.0044	—	—	—		
	CYP2C8	—	—	—	—	—	55.2	—	—		

[a]V_{max} for UGT metabolism is reported as picomole per minute per milligram protein and for CYP metabolism is picomole per minute per milligram protein.
[b]Ertugliflozin unbound fraction ($f_{u,inc}$) in rhCYP 3A4 was 0.81 for 0.11 mg/ml protein concentration, 0.11 in HLMs with 2% BSA, 0.76 for 0.16 mg/ml rhCYP 3A5, 0.90 for 0.06 mg/ml protein rhCYP 2C8.
[c]UGT1A9 and UGT2B7 RAFs were generated using mycophenolic acid and zidovudine as probe substrates, respectively.
[d]CYP3A4 CL_{int} ISEF was 0.12 and the CYP abundance was 137 pmol/mg. The CYP2C8 CL_{int} ISEF was 2.3 and CYP abundance was 24 pmol/mg. An ISEF is not available for CYP3A5.
[e]The f_m by enzyme family is based on combined CYP and UGT $CL_{int,sc,u}$.
[f]M1 CYP2C8 $CL_{int,u}$ was determined by slope of formation since solubility prevented determination of individual kinetic parameters.

per kilogram, with CYPs 3A4 (7.18 ml/min per kilogram) and 2C8 (0.0828 ml/min per kilogram) representing a f_m of 0.99 and 0.01, respectively (Table 4).

Clearance of Ertugliflozin in HLMs and HKMs at 1 μM Ertugliflozin. Ertugliflozin clearance was investigated in HLMs and HKMs in the presence of combined and individual UGT and CYP cofactors. As measured by substrate depletion, the scaled unbound human intrinsic clearance ($CL_{int,sc,u}$) obtained from incubations in HLMs and HKMs was 27.1 and 2.93 ml/min per kilogram, respectively (Table 6), resulting in a combined $CL_{int,sc,u}$ of 30.0 ml/min per kilogram. The resulting f_{CL} was 0.90 and 0.10 for liver and kidney, respectively.

Metabolite formation kinetic analyses after ertugliflozin incubation in HLMs were also conducted to measure $CL_{int,u}$ with individual UGT and CYP cofactors. The HLM UGT-mediated $CL_{int,sc,u}$ was 33.9 ml/min per kilogram, and the CYP mediated $CL_{int,sc,u}$ was 1.55 ml/min per kilogram. The combined HLM $CL_{int,sc,u}$ was 35.5 ml/min per kilogram. The UGT-mediated $CL_{int,sc,u}$ for HKMs was 3.66 ml/min per kilogram. The combined HLM and HKM $CL_{int,sc,u}$ was 39.2 ml/min per kilogram corresponding to a f_{CL} of 0.91 and 0.09 for liver and kidney, respectively. Using the well stirred model, the systemic clearance (CL_b) was 1.55 ml/min per kilogram, where the f_{CL} for liver and kidney was 0.90 and 0.10, respectively.

Nonspecific Binding of Ertugliflozin in HLMs. Under UGT experimental conditions, the f_u measured in an equilibrium dialysis experiment was 0.54 and 0.11 in HLMs (0.25 mg/ml protein) in the absence and presence of 2% BSA, respectively. The $f_{u,HLM}$ at 0.76 mg/ml was 0.397. The fraction unbound for CYP HLM (0.1 mg/ml protein), rhCYP3A4 (0.11 mg/ml protein), rhCYP3A5 (0.16 mg/ml), and rhCYP2C8

TABLE 5

The effect of CYP selective chemical inhibitors on ertugliflozin metabolism in pooled HLMs

Data are expressed as the means from duplicate experiments. The percent inhibition data were scaled to 100% as described under Materials and Methods. The relative contribution values (f_m) were calculated from data scaled to 100% inhibition.

CYP	Inhibitor	M1[a]			M2[a]			M3[a]		
		Rate	Inhibition (scaled to 100%)	f_{mCYP}[b]	Rate	Inhibition (scaled to 100%)	f_{mCYP}[b]	Rate	Inhibition (scaled to 100%)	f_{mCYP}[b]
		$pmol \cdot min^{-1} \cdot mg^{-1}$	%		$pmol \cdot min^{-1} \cdot mg^{-1}$	%		$pmol \cdot min^{-1} \cdot mg^{-1}$	%	
HLM	Control (no preincubation)	7.02	—	—	2.05	—	—	5.51	—	—
2C8	0.64 μM montelukast	6.04	13.9	—	1.54	24.7 (22.1)	0.042	4.51	18.2	—
2C9	10 μM sulfaphenazole	6.28	10.4	—	1.82	11.1	—	4.81	12.7	—
2C19	3 μM benzylnirvanol	7.58	−8.01	—	2.34	−14.4	—	7.14	−29.7	—
2D6	1 μM quinidine	6.75	3.83	—	1.99	3.01	—	5.74	−4.18	—
3A4/5	1 μM ketoconazole	0.569	91.9 (100)	0.72	0.271	86.8 (77.9)	0.15	<1.00	>81.8 (100)	>0.080
HLM	Control (with preincubation)	5.79	—	—	1.66	—	—	4.52	—	—
1A2	10 μM furafylline	6.17	−6.57	—	1.66	0.200	—	4.96	−9.66	—
2B6	3 μM PPP	5.97	−3.17	—	1.66	0.200	—	4.34	4.06	—

[a]M1 and M2 were generated from 10 μM ertugliflozin and M3 was generated from 50 μM ertugliflozin.
[b]Values reported only for those inhibitors that resulted in a statically significant change in rate compare with solvent control ($P < 0.01$).

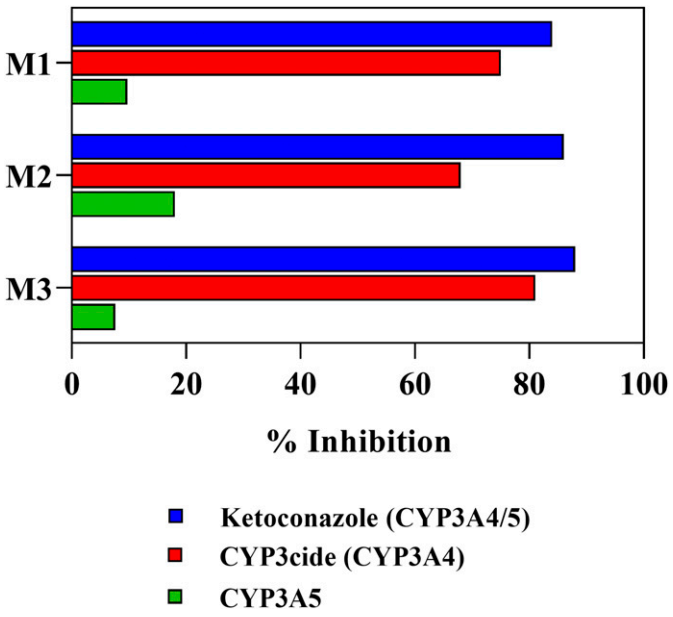

Fig. 5. Percent inhibition of CYP metabolites M1, M2, and M3 by ketoconazole (CYP3A4/5) and CYP3cide (CYP3A4) in pooled HLM 3A4 *1*1 microsomes. CYP3A5 contribution was calculated as the difference between ketoconazole and CYP3cide inhibition. The percent inhibition was used to calculate CYP3A4 and CYP3A5 contributions to M1, M2, and M3 formation (Fig. 6). Mean data represent duplicate incubations.

(0.06 mg/ml protein), were calculated as 0.83, 0.81, 0.76, and 0.90, respectively, using the differential protein binding equation (Austin et al., 2002).

Discussion

Ertugliflozin ADME characterized in a human [^{14}C] mass-balance study demonstrated the primary clearance mechanism was UGT-mediated metabolism (86%) with minor contributions from CYP-mediated metabolism (12%) and renal clearance (2%) (Miao et al., 2013). Reaction phenotyping studies reported herein defined UGT1A9 as the primary enzyme responsible for ertugliflozin metabolic CL with minor contributions from UGT2B7, UGT2B4, CYP3A4, CYP3A5, and CYP2C8. Quantitative UGT reaction phenotyping has advanced significantly (Miners et al., 2010; Zientek and Youdim, 2015; Di, 2017), allowing consistent approaches to conduct core in vitro UGT and CYP phenotyping experiments (Zhang et al., 2007; Miners et al., 2010; Zientek and Youdim, 2015; Di, 2017). Core studies involved identification of human relevant metabolites from elimination routes, defining f_{CL} from enzyme kinetics, qualitative rhUGT mapping, and quantitative detailing with isoform-selective chemical inhibitors to define in vitro f_m. Orthogonal phenotyping approaches informed core studies, which involved scaling recombinant enzyme kinetics (quantitative assessment) using RAF or ISEF, and genotyped tissue fraction studies (i.e., CYP3A5). Based on consistent and robust results defining glucuronidation and UGT1A9 as the primary metabolic enzyme, UGT correlation analyses (Achour et al., 2017) were not pursued.

Human relevant metabolites (Fig. 1) initially identified in human hepatocyte incubations (Kalgutkar et al., 2011) and quantified from human mass-balance studies included three primary regioisomer glucuronides (M5a, M5b, M5c) with M5c representing >80% of UGT-mediated CL (Kalgutkar et al., 2011; Miao et al., 2013). The minor glucuronide (M5b) accounted for <5% of human glucuronidation and was not formed in appreciable amounts in rhUGTs or HLMs to conduct phenotyping. UGT reaction phenotyping of the two primary glucuronides (M5c and M5a), representing >95% of human glucuronidation, was conducted. Oxidative metabolism resulted in elimination of three primary metabolites (M1, M2, M3) and secondary glucuronides (M6a, M6b), assumed secondary to oxidative metabolism, which collectively accounts for a minor (12%) human CL route.

Enzyme kinetic assays defining f_{CL} were conducted in HLMs since UGT-selective chemical inhibitors are not qualified for use in human hepatocytes. HLM formation kinetics for M5c (major) and M5a (minor) were performed with 2% BSA to sequester fatty acids released during microsomal incubations since fatty acids could inhibit activity for some UGT isoforms (e.g., UGT1A9 and UGT2B7), lowering the unbound K_m and hence increasing $CL_{int,u}$ (Rowland et al., 2007; Manevski et al., 2011; Walsky et al., 2012; Miners et al., 2017). Ertugliflozin UGT-mediated $CL_{int,u}$ (9.59 μl/min per milligram) increased 3.9-fold (37.0 μl/min per milligram) in the presence of 2% BSA, primarily driven by a lower unbound K_m with BSA (Table 1), similar to UGT1A9 substrates propofol and mycophenolic acid (Rowland et al., 2008; Gill et al., 2012) or UGT2B7 substrates zidovudine (Manevski et al., 2011; Walsky et al., 2012) and naloxone (Kilford et al., 2009; Gill et al., 2012). In vitro formation of M5c (34.7 μl/min per milligram) was approximately 15-fold greater than M5a (2.28 μl/min per milligram), consistent with human disposition studies indicating M5c as the major human glucuronide (Miao et al., 2013). In vitro formation of oxidative metabolites (1.64 μl/min per milligram) was significantly lower than

TABLE 6

Ertugliflozin (1 μM) clearance estimates and fraction of clearance in HLMs and HKMs by both substrate depletion and metabolite formation

Data are presented as the means of two replicate experiments.

Tissue fraction	Substrate depletion[a,b]				Metabolite formation[b,c]					
	$t_{1/2}$ min	$CL_{int,u}$ μl·min^{-1}·mg^{-1}	$CL_{int,sc,u}$ ml·min^{-1}·kg^{-1}	f_{CL} by Tissue	UGT $CL_{int,sc,u}$ ml·min^{-1}·kg^{-1}	CYP $CL_{int,sc,u}$ ml·min^{-1}·kg^{-1}	Total $CL_{int,sc,u}$ ml·min^{-1}·kg^{-1}	f_{CL} by Tissue	CL_b[d] ml·min^{-1}·kg^{-1}	Systemic f_{CL}
HLM	110	28.6	27.1	0.90	5.02[e], 28.9[f]	1.55	35.5	0.91	2.97	0.90
HKM	62.0	50.8	2.93	0.10	—[e], 3.66[f]	—	3.66	0.09	0.348	0.10
Combined	—		30.0	1.00	—	—	39.2	1.00	3.32	1.00

$t_{1/2}$, half-life.
[a]Clearance by substrate depletion was determined in the presence of combined cofactors for UGT and CYP metabolism.
[b]Substrate depletion and UGT metabolite formation experiments were conducted in the presence of 2% BSA.
[c]Clearance estimates by metabolite formation were determined in the presence of individual cofactors.
[d]CL_b scaled with well stirred liver or kidney model using blood flow of 20 and 18 ml/min per kilogram, respectively, $f_{u,p}$ of 0.064, and C_B/C_P of 0.66.
[e]Value represents formation of M5a scaled from ertugliflozin concentration of 1 μM in HLMs and HKMs. The HLM value is comparable to full enzyme kinetic clearance (2.15 ml/min per kilogram) as presented in Table 1.
[f]Value represents formation of M5c scaled from ertugliflozin concentration of 1 μM in HLMs and HKMs. The HLM value is comparable to full enzyme kinetic clearance (32.8 ml/min per kilogram) as presented in Table 1.

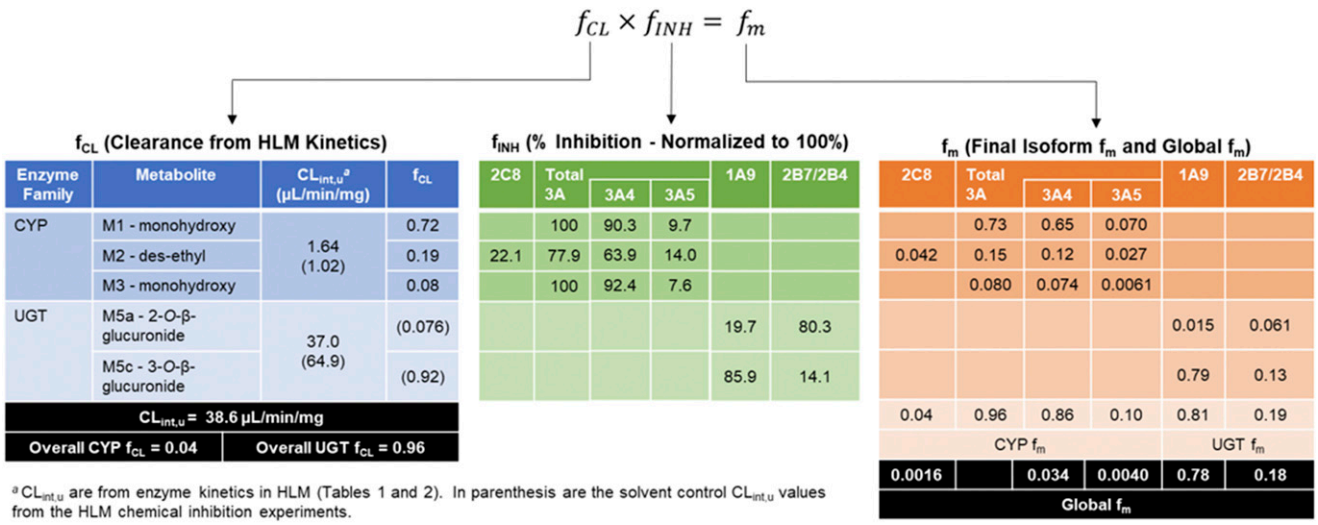

Fig. 6. Ertugliflozin global in vitro hepatic f_m estimated from UGT- and CYP-mediated f_{CL} and fraction of metabolism inhibited (f_{inh}) after incubation with isoform-selective chemical inhibitors.

glucuronidation, resulting in f_{CL} estimates of hepatic glucuronidation versus oxidative metabolism of 96% and 4%, respectively. These f_{CL} estimates predict major human conjugative CL mechanisms well (88%) when not accounting for renal CL, and somewhat underestimate observed human oxidative CL (12%). A possible explanation for the underestimation of observed human oxidative CL is the potential reabsorption of ertugliflozin, which is generated from hydrolysis of biliary secreted ertugliflozin glucuronides in the gastrointestinal tract. The potential reabsorption and subsequent metabolism by CYP3A4 in the intestine may account for the increased contribution of oxidative metabolism to ertugliflozin metabolism in vivo, resulting in an underestimation of CYP-mediated metabolism using in vitro studies. However, a physiologically based pharmacokinetic model for ertugliflozin, which does not contain this reabsorption component, adequately characterizes ertugliflozin pharmacokinetics across a dose range of 0.5–300 mg, indicating that any potential reabsorption does not significantly contribute to ertugliflozin disposition and the role of oxidative metabolism in ertugliflozin metabolism remains small (Callegari et al., 2020).

Qualitative recombinant UGT enzyme mapping identified UGT1A9 as the apparent major enzyme responsible for M5c glucuronide formation, whereas extrahepatic UGTs 1A7 and 1A8 also demonstrated catalytic turnover (Fig. 4). At higher concentrations, formation of M5c was also catalyzed by UGT1A3 and UGT2B7, albeit at apparently low turnover rates. In addition to UGT1A9, subsequent kinetic experiment with rhUGTs (Table 4) and chemical inhibition studies (Table 3) indicated a minor but more substantial role for UGT2B7 in M5c glucuronidation (Fig. 2). This increase in CL_{int} is likely due to the inclusion of 2% BSA in rhUGT kinetic assays and HLM chemical inhibitor studies, which have demonstrated significant increases in rhUGT CL_{int} (9-fold) for UGT2B7 substrates such as zidovudine (Walsky et al., 2012). In turn, M5a glucuronidation was apparently primarily catalyzed by UGTs 1A9, 2B7, and 2B4 (Fig. 4) with low turnover rates from other UGT1A enzymes. Subsequent phenotyping studies demonstrated a more significant contribution of UGT2B7 relative to UGT1A9 than apparent from rhUGT mapping.

Quantitative chemical inhibition studies conducted in the presence of digoxin and tranilast (Lapham et al., 2012) demonstrated that UGT1A9 (f_m 0.81) is the primary enzyme responsible for ertugliflozin glucuronidation, whereas the minor route (f_m 0.19) was assigned to UGT2B7 and UGT2B4 after incubation with 16β-phenyllongifolol (Bichlmaier et al., 2007; Lapham et al., 2012). Although 16β-phenyllongifolol was previously considered a selective inhibitor of UGT2B7, recent development of a selective UGT2B4 substrate assay in HLMs in our laboratory demonstrated that 16β-phenyllongifolol (3 μM) is a nonselective inhibitor against UGT2B7 and UGT2B4 substrates resulting in >90% inhibition (unpublished data). Quantitative proteomics could provide insight into the potential contribution of UGTs 2B4 and 2B7 toward ertugliflozin minor glucuronidation route (f_m 0.19). Expression of UGT2B4 (picomole per milligram protein) in pooled HLMs is approximately 50% lower than UGT2B7 (Fallon et al., 2013b; Achour et al., 2017). Since 16β-phenyllongifolol completely inhibited UGTs 2B4 and 2B7 activity in HLMs and assuming that UGT2B4 and UGT2B7 HLM enzyme kinetic parameters for ertugliflozin glucuronidation are similar, one-third of UGT2B ertugliflozin glucuronidation could be assigned to UGT2B4 (f_m 0.06) and two-thirds to UGT2B7 (f_m 0.13).

Orthogonal assays were also employed to substantiate or inform UGT chemical inhibition phenotyping based on increasing evidence of successful RAF scaling of rhUGT CL_{int} to HLMs with utility in UGT prototyping (Rouguieg et al., 2010; Zhu et al., 2012). Scaling of rhUGT CL_{int} for UGTs 1A9 and 2B7 provided very similar estimates of relative in vitro f_m (0.86 vs. 0.14) compared with chemical inhibition (0.81 vs. 0.19). Although not the focus of this study, it is of interest that the RAF-adjusted in vivo CL_{int} for glucuronidation (22.7 ml/min per kilogram) was within 2-fold or approximately 0.65-fold the HLM glucuronidation CL_{int} (34.9 ml/min per kilogram).

Since UGT1A9 and UGT2B7 are the primary and secondary respective UGTs expressed in human kidney (Fallon et al., 2013a; Zientek and Youdim, 2015), it is important to consider extrahepatic metabolic CL for ertugliflozin. Because ertugliflozin is not subject to significant intestinal first-pass metabolic extraction (F_g 0.98) (Callegari et al., 2020) and UGT1A9 expression level in the intestine is very low or undetectable (Fallon et al., 2013a; Zientek and Youdim, 2015), in vitro intestinal metabolism was not investigated. As anticipated, ertugliflozin in vitro CL_{int} was higher in HKMs compared with HLMs since relative UGT1A9 expression (picomole per milligram tissue) is approximately 2- to 3-fold higher (Mukai et al., 2014; Zientek and Youdim, 2015). However, CL_{int} scaled for tissue CL is approximately 10-fold lower for human kidney relative to liver, primarily due to the differences in organ

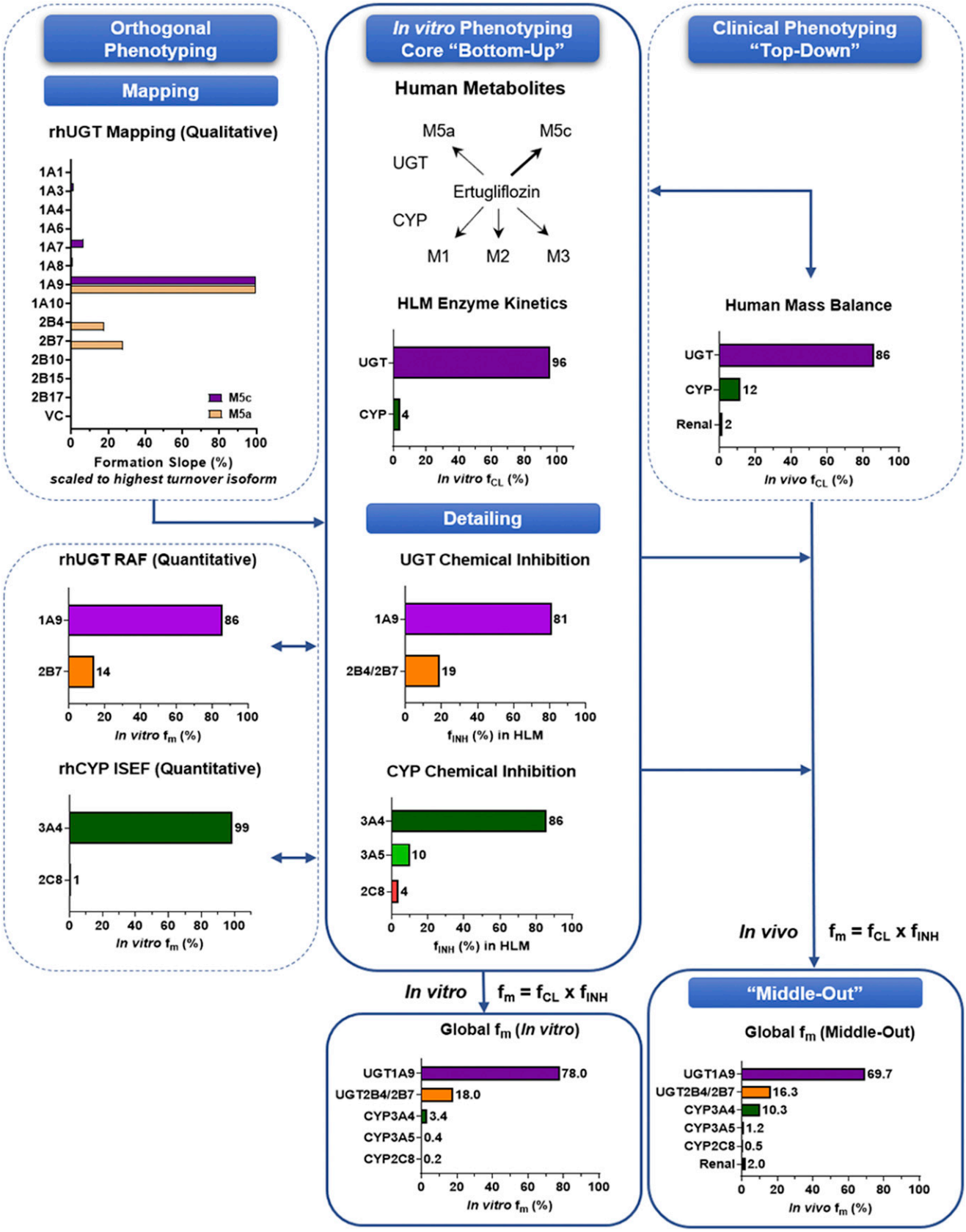

Fig. 7. Integration of "bottom-up" core in vitro phenotyping and orthogonal studies to establish in vitro f_m and "middle-out" in vivo f_m for ertugliflozin based on "top-down" human mass balance disposition. [Adapted from Figure 7 (Minors et al., 2020)]

weight. Only the UGT1A9 metabolite (M5c) was quantifiable in HKMs, in line with relative f_m UGT for ertugliflozin and expression levels of UGTs 1A9 and 2B7 (Fallon et al., 2013a; Margaillan et al., 2015), whereas oxidative metabolism was not observed (Table 6). Similar results for UGT1A9 substrate propofol demonstrated V_{max} and CL_{int} were 2.1- and 3.7-fold higher in HKMs relative to HLMs (Mukai et al., 2014). It is therefore anticipated that kidney metabolic CL will account for approximately 10% of total systemic ertugliflozin CL, primarily mediated by UGT1A9.

Minor oxidative CL routes (<20%) could prove important during physiologically based pharmacokinetic model development, particularly when assessing CYP3A4-mediated enzyme induction for victim drugs (Gandelman et al., 2011). Chemical inhibition studies demonstrated most of the ertugliflozin oxidative metabolism was mediated by CYP3A (96%) with a small contribution by CYP2C8 (0%–4%). Utilizing chemical inhibition studies in genotyped CYP3A5 tissue fractions (Tseng et al., 2014), it was evident that CYP3A4 (f_m 0.86–1.0) was responsible for the majority of CYP3A (f_m 0.96) mediated metabolism, relative to CYP3A5 (f_m 0–0.1) (Fig. 6). Orthogonal ISEF-adjusted scaling of rhCYP3A4 and CYP2C8 CL_{int} suggested a lessor role of CYP2C8 (f_m 0.01) relative to CYP3A4 (f_m 0.99). The increased relative contribution of CYP3A is apparently due to the tendency of ISEF-adjusted rhP450 CL_{int} to overestimate CYP3A-mediated CL relative to other CYP enzymes (Chen et al., 2011; Umehara et al., 2017; Lindmark et al., 2018).

In conclusion, UGT1A9 is the primary enzyme responsible for ertugliflozin metabolic CL, consistent with the major clearance routes identified for structurally related SGLT2 inhibitors such as dapagliflozin (Kasichayanula et al., 2013) and canagliflozin (Mamidi et al., 2014; Devineni and Polidori, 2015). A "bottom-up" in vitro reaction phenotyping approach (Fig. 7) defined UGT1A9 (f_m 78%) as the major enzyme responsible for ertugliflozin hepatic CL with minor contributions from UGT2B7/UGT2B4 (f_m 18%), CYP3A4 (f_m 3.4%), CYP3A5 (f_m 0.4%), and CYP2C8 (f_m 0.16%). "Top-down" integration of higher observed clinical ertugliflozin oxidative disposition (12% vs. 4%) and renal elimination (Miao et al., 2013) would result in "middle-out" altered in vivo human f_m values for UGT1A9 (f_m 69.7%), UGT2B7/UGT2B4 (f_m 16.3%), CYP3A4 (f_m 10.3%), CYP3A5 (f_m 1.2%), and CYP2C8 (f_m 0.16%). These findings enabled physiologically based pharmacokinetic drug-drug interaction risk assessment with Simcyp using ertugliflozin coadministered with UGT1A9 inhibitor mefenamic acid (Callegari et al., 2020) and could be used for further interpretation of ertugliflozin disposition and drug-drug interaction risk assessment with coadministered drugs.

Authorship Contributions

Participated in research design: Lapham, Callegari, Cianfrogna, Lin, Goosen.

Conducted experiments: Lapham, Cianfrogna, Lin, Niosi, Orozco, Sharma.

Performed data analysis: Lapham, Cianfrogna, Lin, Niosi, Orozco, Sharma, Goosen

Wrote or contributed to the writing of the manuscript: Lapham, Callegari, Cianfrogna, Lin, Goosen.

Note Added in Proof: During the proof stage, several errors were discovered, the center table heading was cutoff in Figure 6 and a permission statement was accidentally not included in Figure 7 caption of the Fast Forward version that appeared online October 5, 2020. Figure 6 and Figure 7 caption have been corrected.

References

Achour B, Dantonio A, Niosi M, Novak JJ, Fallon JK, Barber J, Smith PC, Rostami-Hodjegan A, and Goosen TC (2017) Quantitative characterization of major hepatic UDP-glucuronosyltransferase enzymes in human liver microsomes: comparison of two proteomic methods and correlation with catalytic activity. *Drug Metab Dispos* **45**:1102–1112.

Austin RP, Barton P, Cockroft SL, Wenlock MC, and Riley RJ (2002) The influence of nonspecific microsomal binding on apparent intrinsic clearance, and its prediction from physicochemical properties. *Drug Metab Dispos* **30**:1497–1503.

Bichlmaier I, Kurkela M, Joshi T, Siiskonen A, Rüffer T, Lang H, Finel M, and Yli-Kauhaluoma J (2007) Potent inhibitors of the human UDP-glucuronosyltransferase 2B7 derived from the sesquiterpenoid alcohol longifolol. *ChemMedChem* **2**:881–889.

Callegari E, Lin J, Tse S, Goosen TC, and Sahasrabudhe V (2020) Physiologically based pharmacokinetic modeling of drug–drug interaction of the UGT substrate ertugliflozin following coadministration with the UGT inhibitor mefenamic acid. *CPT Pharmacometrics Syst Pharmacol*, in press.

Chen Y, Liu L, Nguyen K, and Fretland AJ (2011) Utility of intersystem extrapolation factors in early reaction phenotyping and the quantitative extrapolation of human liver microsomal intrinsic clearance using recombinant cytochromes P450. *Drug Metab Dispos* **39**:373–382.

Deeks ED and Scheen AJ (2017) Canagliflozin: a review in type 2 diabetes. *Drugs* **77**:1577–1592.

Devineni D and Polidori D (2015) Clinical pharmacokinetic, pharmacodynamic, and drug-drug interaction profile of canagliflozin, a sodium-glucose co-transporter 2 inhibitor. *Clin Pharmacokinet* **54**:1027–1041.

Di L (2017) Reaction phenotyping to assess victim drug-drug interaction risks. *Expert Opin Drug Discov* **12**:1105–1115.

Di L, Umland JP, Trapa PE, and Maurer TS (2012) Impact of recovery on fraction unbound using equilibrium dialysis. *J Pharm Sci* **101**:1327–1335.

Fallon JK, Neubert H, Goosen TC, and Smith PC (2013a) Targeted precise quantification of 12 human recombinant uridine-diphosphate glucuronosyl transferase 1A and 2B isoforms using nano-ultra-high-performance liquid chromatography/tandem mass spectrometry with selected reaction monitoring. *Drug Metab Dispos* **41**:2076–2080.

Fallon JK, Neubert H, Hyland R, Goosen TC, and Smith PC (2013b) Targeted quantitative proteomics for the analysis of 14 UGT1As and -2Bs in human liver using NanoUPLC-MS/MS with selected reaction monitoring. *J Proteome Res* **12**:4402–4413.

Frampton JE (2018) Empagliflozin: a review in type 2 diabetes. *Drugs* **78**:1037–1048.

Freitas HS, Anhê GF, Melo KF, Okamoto MM, Oliveira-Souza M, Bordin S, and Machado UF (2008) Na(+) -glucose transporter-2 messenger ribonucleic acid expression in kidney of diabetic rats correlates with glycemic levels: involvement of hepatocyte nuclear factor-1alpha expression and activity. *Endocrinology* **149**:717–724.

Gandelman K, Zhu T, Fahmi OA, Glue P, Lian K, Obach RS, and Damle B (2011) Unexpected effect of rifampin on the pharmacokinetics of linezolid: in silico and in vitro approaches to explain its mechanism. *J Clin Pharmacol* **51**:229–236.

Ghezzi C and Wright EM (2012) Regulation of the human Na+-dependent glucose cotransporter hSGLT2. *Am J Physiol Cell Physiol* **303**:C348–C354.

Gill KL, Houston JB, and Galetin A (2012) Characterization of in vitro glucuronidation clearance of a range of drugs in human kidney microsomes: comparison with liver and intestinal glucuronidation and impact of albumin. *Drug Metab Dispos* **40**:825–835.

Han S, Hagan DL, Taylor JR, Xin L, Meng W, Biller SA, Wetterau JR, Washburn WN, and Whaley JM (2008) Dapagliflozin, a selective SGLT2 inhibitor, improves glucose homeostasis in normal and diabetic rats. *Diabetes* **57**:1723–1729.

Hollander P, Hill J, Johnson J, Wei Jiang Z, Golm G, Huyck S, Terra SG, Mancuso JP, Engel SS, Lauring B, et al. (2019) Results of VERTIS SU extension study: safety and efficacy of ertugliflozin treatment over 104 weeks compared to glimepiride in patients with type 2 diabetes mellitus inadequately controlled on metformin. *Curr Med Res Opin* **35**:1335–1343.

Hummel CS, Lu C, Loo DD, Hirayama BA, Voss AA, and Wright EM (2011) Glucose transport by human renal Na+/D-glucose cotransporters SGLT1 and SGLT2. *Am J Physiol Cell Physiol* **300**: C14–C21.

Kalgutkar AS, Tugnait M, Zhu T, Kimoto E, Miao Z, Mascitti V, Yang X, Tan B, Walsky RL, Chupka J, et al. (2011) Preclinical species and human disposition of PF-04971729, a selective inhibitor of the sodium-dependent glucose cotransporter 2 and clinical candidate for the treatment of type 2 diabetes mellitus. *Drug Metab Dispos* **39**:1609–1619.

Kasichayanula S, Liu X, Griffen SC, Lacreta FP, and Boulton DW (2013) Effects of rifampin and mefenamic acid on the pharmacokinetics and pharmacodynamics of dapagliflozin. *Diabetes Obes Metab* **15**:280–283.

Kilford PJ, Stringer R, Sohal B, Houston JB, and Galetin A (2009) Prediction of drug clearance by glucuronidation from in vitro data: use of combined cytochrome P450 and UDP-glucuronosyltransferase cofactors in alamethicin-activated human liver microsomes. *Drug Metab Dispos* **37**:82–89.

Lapham K, Bauman JN, Walsky RL, Niosi M, Orozco CO, Bourcier K, Giddens G, Obach RS, Hyland R, and Goosen TC (2012) P108. Digoxin and tranilast identified as novel isoform-selective inhibitors of human UDP-glucuronosyltransferase 1A9 (UGT1A9) activity. *Drug Metab Rev* **44** (Suppl 1):82.

Lin J, Dantonio AL, Lapham K, Niosi M, Orozco CO, Callegari E, Leung LY, and Goosen TC (2015) P209. In vitro-in vivo extrapolation of UGT1A9-mediated clearance and application in a PBPK model for dapagliflozin. *Drug Metab Rev* **47** (Suppl 1):1–313.

Lin J, Lapham K, Niosi M, Orozco CO, Fallon JK, Neubert H, Smith PC, Rahavendran R, Leung LY, and Goosen TC (2014) P57. Intersystem extrapolation factors (ISEF) for human UDP-glucuronosyltransferase (UGT) activity: utility to estimate UGT1A1-mediated fractional clearance. *Drug Metab Rev* **45** (Suppl 1):62–63.

Lindmark B, Lundahl A, Kanebratt KP, Andersson TB, and Isin EM (2018) Human hepatocytes and cytochrome P450-selective inhibitors predict variability in human drug exposure more accurately than human recombinant P450s. *Br J Pharmacol* **175**:2116–2129.

Mamidi RN, Cuyckens F, Chen J, Scheers E, Kalamaridis D, Lin R, Silva J, Sha S, Evans DC, Kelley MF, et al. (2014) Metabolism and excretion of canagliflozin in mice, rats, dogs, and humans. *Drug Metab Dispos* **42**:903–916.

Manevski N, Moreolo PS, Yli-Kauhaluoma J, and Finel M (2011) Bovine serum albumin decreases Km values of human UDP-glucuronosyltransferases 1A9 and 2B7 and increases Vmax values of UGT1A9. *Drug Metab Dispos* **39**:2117–2129.

Margaillan G, Rouleau M, Fallon JK, Caron P, Villeneuve L, Turcotte V, Smith PC, Joy MS, and Guillemette C (2015) Quantitative profiling of human renal UDP-glucuronosyltransferases and glucuronidation activity: a comparison of normal and tumoral kidney tissues. *Drug Metab Dispos* **43**:611–619.

Markham A (2018) Ertugliflozin: first global approval. *Drugs* **78**:513–519.

Mascitti V, Maurer TS, Robinson RP, Bian J, Boustany-Kari CM, Brandt T, Collman BM, Kalgutkar AS, Klenotic MK, Leininger MT, et al. (2011) Discovery of a clinical candidate from the structurally unique dioxa-bicyclo[3.2.1]octane class of sodium-dependent glucose cotransporter 2 inhibitors. *J Med Chem* **54**:2952–2960.

Miao Z, Nucci G, Amin N, Sharma R, Mascitti V, Tugnait M, Vaz AD, Callegari E, and Kalgutkar AS (2013) Pharmacokinetics, metabolism, and excretion of the antidiabetic agent ertugliflozin (PF-04971729) in healthy male subjects. *Drug Metab Dispos* **41**:445–456.

Miners JO, Chau N, Rowland A, Burns K, McKinnon RA, Mackenzie PI, Tucker GT, Knights KM, and Kichenadasse G (2017) Inhibition of human UDP-glucuronosyltransferase enzymes by lapatinib, pazopanib, regorafenib and sorafenib: implications for hyperbilirubinemia. *Biochem Pharmacol* **129**:85–95.

Miners JO, Mackenzie PI, and Knights KM (2010) The prediction of drug-glucuronidation parameters in humans: UDP-glucuronosyltransferase enzyme-selective substrate and inhibitor probes for reaction phenotyping and in vitro-in vivo extrapolation of drug clearance and drug-drug interaction potential. *Drug Metab Rev* **42**:196–208.

Minors John O, Rowland Andrew, Novak Jonathan J, Lapham Kimberly, and Goosen Theunis C. (2020) Evidence-based strategies for the characterisation of human drug and chemical glucuronidation in vitro and UDP-glucuronosyltransferase reaction phenotyping. *Pharmacology & Therapeutics*, doi: https://doi.org/10.1016/j.pharmthera.2020.107689 In press.

Mukai M, Tanaka S, Yamamoto K, Murata M, Okada K, Isobe T, Shigeyama M, Hichiya H, and Hanioka N (2014) In vitro glucuronidation of propofol in microsomal fractions from human liver, intestine and kidney: tissue distribution and physiological role of UGT1A9. *Pharmazie* **69**:829–832.

Plosker GL (2014) Dapagliflozin: a review of its use in patients with type 2 diabetes. *Drugs* **74**: 2191–2209.

Raje S, Callegari E, Sahasrabudhe V, Vaz A, Shi H, Fluhler E, Woolf EJ, Schildknegt K, Matschke K, Alvey C, et al. (2018) Novel application of the two-period microtracer approach to determine absolute oral bioavailability and fraction absorbed of ertugliflozin. *Clin Transl Sci* **11**:405–411.

Rouguieg K, Picard N, Sauvage FL, Gaulier JM, and Marquet P (2010) Contribution of the different UDP-glucuronosyltransferase (UGT) isoforms to buprenorphine and norbuprenorphine metabolism and relationship with the main UGT polymorphisms in a bank of human liver microsomes. *Drug Metab Dispos* **38**:40–45.

Rowland A, Gaganis P, Elliot DJ, Mackenzie PI, Knights KM, and Miners JO (2007) Binding of inhibitory fatty acids is responsible for the enhancement of UDP-glucuronosyltransferase 2B7 activity by albumin: implications for in vitro-in vivo extrapolation. *J Pharmacol Exp Ther* **321**: 137–147.

Rowland A, Knights KM, Mackenzie PI, and Miners JO (2008) The "albumin effect" and drug glucuronidation: bovine serum albumin and fatty acid-free human serum albumin enhance the glucuronidation of UDP-glucuronosyltransferase (UGT) 1A9 substrates but not UGT1A1 and UGT1A6 activities. *Drug Metab Dispos* **36**:1056–1062.

Tentolouris A, Vlachakis P, Tzeravini E, Eleftheriadou I, and Tentolouris N (2019) SGLT2 inhibitors: a review of their antidiabetic and cardioprotective effects. *Int J Environ Res Public Health* **16**:2965.

Terra SG, Focht K, Davies M, Frias J, Derosa G, Darekar A, Golm G, Johnson J, Saur D, Lauring B, et al. (2017) Phase III, efficacy and safety study of ertugliflozin monotherapy in people with type 2 diabetes mellitus inadequately controlled with diet and exercise alone. *Diabetes Obes Metab* **19**:721–728.

Tseng E, Walsky RL, Luzietti RA Jr, Harris JJ, Kosa RE, Goosen TC, Zientek MA, and Obach RS (2014) Relative contributions of cytochrome CYP3A4 versus CYP3A5 for CYP3A-cleared drugs assessed in vitro using a CYP3A4-selective inactivator (CYP3cide). *Drug Metab Dispos* **42**:1163–1173.

Umehara KI, Huth F, Gu H, Schiller H, Heimbach T, and He H (2017) Estimation of fractions metabolized by hepatic CYP enzymes using a concept of inter-system extrapolation factors (ISEFs) - a comparison with the chemical inhibition method. *Drug Metab Pers Ther* **32**:191–200.

Vrhovac I, Balen Eror D, Klessen D, Burger C, Breljak D, Kraus O, Radović N, Jadrijević S, Aleksic I, Walles T, et al. (2015) Localizations of Na(+)-D-glucose cotransporters SGLT1 and SGLT2 in human kidney and of SGLT1 in human small intestine, liver, lung, and heart. *Pflugers Arch* **467**:1881–1898.

Walsky RL, Bauman JN, Bourcier K, Giddens G, Lapham K, Negahban A, Ryder TF, Obach RS, Hyland R, and Goosen TC (2012) Optimized assays for human UDP-glucuronosyltransferase (UGT) activities: altered alamethicin concentration and utility to screen for UGT inhibitors. *Drug Metab Dispos* **40**:1051–1065.

Wright EM (2001) Renal Na(+)-glucose cotransporters. *Am J Physiol Renal Physiol* **280**:F10–F18.

Zhang H, Davis CD, Sinz MW, and Rodrigues AD (2007) Cytochrome P450 reaction-phenotyping: an industrial perspective. *Expert Opin Drug Metab Toxicol* **3**:667–687.

Zhu L, Ge G, Zhang H, Liu H, He G, Liang S, Zhang Y, Fang Z, Dong P, Finel M, et al. (2012) Characterization of hepatic and intestinal glucuronidation of magnolol: application of the relative activity factor approach to decipher the contributions of multiple UDP-glucuronosyltransferase isoforms. *Drug Metab Dispos* **40**:529–538.

Zientek MA and Youdim K (2015) Reaction phenotyping: advances in the experimental strategies used to characterize the contribution of drug-metabolizing enzymes. *Drug Metab Dispos* **43**: 163–181.

Address correspondence to: Kimberly Lapham, Medicine Design, Pfizer Inc, Eastern Point Rd., Groton, CT 06340. E-mail: kimberly.lapham@pfizer.com